Received: 19 March 2024 | Revised: 7 May 2024 | Accepted: 16 May 2024

DOI: 10.1111/acel.14235

Aging Cell WILEY

RESEARCH ARTICLE

# Metformin treatment results in distinctive skeletal muscle mitochondrial remodeling in rats with different intrinsic aerobic capacities

Matthew P. Bubak[1] | Arik Davidyan[1,2] | Colleen L. O'Reilly[1] | Samim A. Mondal[1] | Jordan Keast[1] | Stephen M. Doidge[1] | Agnieszka K. Borowik[1] | Michael E. Taylor[1] | Evelina Volovičeva[1] | Michael T. Kinter[1] | Steven L. Britton[3,4] | Lauren G. Koch[5] | Michael B. Stout[1] | Tommy L. Lewis Jr[1] | Benjamin F. Miller[1,6]

[1]Aging and Metabolism Research Program, The Oklahoma Medical Research Foundation, Oklahoma City, Oklahoma, USA

[2]Department of Biological Sciences, California State University Sacramento, Sacramento, California, USA

[3]Department of Anesthesiology, University of Michigan, Ann Arbor, Michigan, USA

[4]Department of Molecular & Integrative Physiology, University of Michigan, Ann Arbor, Michigan, USA

[5]Department of Physiology and Pharmacology, College of Medicine and Life Sciences, The University of Toledo, Toledo, Ohio, USA

[6]The Oklahoma VA Medical Center, Oklahoma City, Oklahoma, USA

**Correspondence**
Benjamin F. Miller, Aging and Metabolism Research Program, Oklahoma Medical Research Foundation, 825 NE 13th Street, Oklahoma City, Oklahoma 73104, USA.
Email: benjamin-miller@omrf.org

**Funding information**
National Institute of General Medical Sciences, Grant/Award Number: 5R24GM137786 and R35GM137921; Oklahoma Nathan Shock Center, Grant/Award Number: 5P20GM103447 and 5P30AG050911; National Institutes of Health, Grant/Award Number: T32 AG052363 and P40OD-021331

## Abstract

The rationale for the use of metformin as a treatment to slow aging was largely based on data collected from metabolically unhealthy individuals. For healthspan extension metformin will also be used in periods of good health. To understand the potential context specificity of metformin treatment on skeletal muscle, we used a rat model (high-capacity runner/low-capacity runner [HCR/LCR]) with a divide in intrinsic aerobic capacity. Outcomes of metformin treatment differed based on baseline intrinsic mitochondrial function, oxidative capacity of the muscle (gastroc vs soleus), and the mitochondrial population (intermyofibrillar vs. subsarcolemmal). Metformin caused lower ADP-stimulated respiration in LCRs, with less of a change in HCRs. However, a washout of metformin resulted in an unexpected doubling of respiratory capacity in HCRs. These improvements in respiratory capacity were accompanied by mitochondrial remodeling that included increases in protein synthesis and changes in

**Abbreviations:** ADP, adenosine diphosphate; AMPK, AMP-activated protein kinase; BMI, body mass index; CI, complex I; CII, complex II; CIII, complex III; CIV, complex IV; CON, control; CSA, cross sectional area; CV, complex V; Cyto, cytosolic; $D_2O$, deuterium oxide; EDL, extensor digitorum longus; $E_{precursor}$, enrichment of the precursor; $E_{product}$, enrichment of the produce; ETS, electron transport system; FSR, fractional synthesis rate; G6Pase, Glucose-6-phosphatase; gastroc, gastrocnemius; HCRs, high capacity runners; IMF, intramyofibrillar mitochondria; K[1/day], Synthesis rate; LCRs, low capacity runners; MET, metformin; Met-Spike, metfomrin spike; MET-WO, metformin washout; MFF, mitochondrial fission factor; MFN1, Mitofusin 1; MFN2, Mitofusin 2; Mito, mitochondrial; Myo, myofibrillar; OPA1, mitocondrial dynamic like GTPase; Oxphos, oxidative phosphorylation; P/E, oxphos to electron transport ratio; PEPCK, Phosphoenolpyruvate carboxykinase; QMR, quantitative magnetic resonance; SE, Standard error; SS, subsarcolemmal mitochondria; T2D, type II diabetes; TA, tibialis anterior; TAME, Targeting Ageing with Metformin; $V_{max}$, maximal respiration.

Matthew P. Bubak and Arik Davidyan shared co-first authorship.

morphology. Our findings raise questions about whether the positive findings of metformin treatment are broadly applicable.

**KEYWORDS**
deuterium oxide, geroscience, healthspan, protein synthesis, proteomics

## 1 | INTRODUCTION

Metformin is the most prescribed drug for type 2 diabetes (T2D) and is the fourth most prescribed pharmaceutical in the United States. Metformin has over 50 years of safety data, is cost-effective, and is associated with a decreased risk of mortality and morbidity for diseases such as cardiovascular disease, cancer, and dementia (Chaudhari et al., 2020; Griffin et al., 2017; Li et al., 2018). The beneficial effects of metformin on multiple chronic diseases make it an attractive candidate to slow aging and extend healthspan, which led to the proposed Targeting Ageing with Metformin (TAME) trial (Barzilai et al., 2016). A meta-analysis of clinical trials suggests that people with T2D taking metformin have lower all-cause mortality and cancer incidence than other diabetics and the general population (Campbell et al., 2017). Much has also been made about the observation that metformin-treated (MET) patients with T2D had better survival rates than their matched nondiabetic control (CON) group (Bannister et al., 2014). However, a recent study that followed individuals who take metformin for 20 years showed that T2D patients had shorter survival than controls (Stevenson-Hoare et al., 2023). The effects of metformin in healthy individuals are less understood.

One accepted definition of healthspan is the period free of chronic disease (Kaeberlein, 2018). To determine if pharmaceuticals can delay the development or progression of age-related chronic diseases, we must introduce the treatment prior to the onset of age-related diseases as once age-related diseases start to accumulate, the healthspan has ended. Slowing the aging process is more likely to be effective than trying to reverse aging once it has occurred as prevention is more effective than reversal (Konopka & Miller, 2019; Miller & Thyfault, 2020). Therefore, treatments, like metformin, which prolong healthspan would start while an individual is healthy and absent of chronic disease. We highlighted that it appears that benefits of metformin are reduced in those without chronic disease (Konopka & Miller, 2019). In the landmark Diabetes Prevention Program, secondary analyses showed that metformin had minimal effects in individuals with a lower BMI (<30 kg/m$^2$) and fasting glucose (<110 mg/dL) (Knowler et al., 2002). Furthermore, a small clinical trial showed that metformin increased insulin sensitivity in subjects with T2D or had a family history of T2D, but worsened insulin sensitivity in other subjects (Iannello et al., 2004). Finally, our previous study (Konopka et al., 2019) and the MASTERS trial (Long et al., 2017) showed that metformin inhibited the positive effects of aerobic or resistance training, respectively, in older healthy individuals. The absence of a positive effect of metformin treatment in healthy individuals is relatively inconsequential, but potential detrimental effects would render metformin treatment untenable. Thus, the efficacy of metformin to extend healthspan in healthy aging populations warrants further investigation.

Surprisingly, the mechanisms of metformin are only partially understood. One proposed action of metformin is a disruption of mitochondrial respiratory capacity through inhibition of complex I (CI) of the electron transport system (ETS) (Brunmair et al., 2004; Wessels et al., 2014) with subsequent activation of AMP-activated protein kinase (AMPK) (Wang et al., 2019). A second potential mechanism results from the positive charge of metformin, which accumulates in the inner mitochondrial membrane space and disrupts mitochondrial membrane potential (Owen et al., 2000). This potential mechanism would result in an inefficiency in energy transfer and active AMPK (Wang et al., 2019). Chronic AMPK activation results in mitochondrial remodeling through protein turnover and fission/fusion events (Toyama et al., 2016) to reestablish energetic homeostasis. Mechanisms of mitochondrial remodeling are energetically costly and result in additional cellular energetic stress. Thus, the ultimate success or failure of the mitochondrial remodeling depends on the energy production and the cellular priorities for energy.

Aerobic capacity (i.e., $VO_{2max}$) is a major predictor of all-cause morbidity and mortality (Blair et al., 1989; Willis et al., 2012). While determinants of aerobic capacity are multifactorial, one important determinant is energy transfer in mitochondria (Okita et al., 1998; Rasmussen et al., 2001). High-capacity and low-capacity running rats (HCRs and LCRs, respectively) are outbred lines generated from a founder population of male and female N:NIH stock rats based on the capacity for energy transfer (i.e., aerobic capacity). Through an intricate breeding program and the selection for the polygenic trait of running capacity, HCRs/LCRs maintain genetic heterogeneity but are differentiated by intrinsic mitochondrial function (Koch & Britton, 2018). Because of this selective breeding over multiple generations, HCRs have greater mitochondrial content, mitochondrial respiration capacity, and $VO_{2max}$ compared to LCRs (Aon et al., 2021; Koch et al., 2012; Koch & Britton, 2001, 2018). Further, LCRs develop diseases such as metabolic syndrome, fatty liver disease, and cancer earlier and more frequently than HCRs and have a decreased lifespan (Koch & Britton, 2001, 2018). Importantly, these differences emerge without exercise training, allowing for the examination of a gain (HCR) or loss (LCR) of intrinsic mitochondrial function independently from exercise-training effects (Fitzgerald et al., 2016). Thus, these rats provide a unique contrasting heterogeneous (noninbred) models for closer translational exploration of aging (Koch et al., 2011), and are an excellent model to test if differences in intrinsic aerobic capacity impact metformin treatment outcomes.

We aimed to test if metformin treatment outcomes depend on intrinsic mitochondrial capacity. The HCR/LCR model allowed us to directly test a biological feature, different intrinsic mitochondrial oxidative capacity, in a genetically heterogeneous model improving translatability to human studies. We treated rats with metformin for 28 days starting at 18-months of age as it equates to middle-age when humans are likely to undergo healthspan-increasing treatments. We primarily focused on skeletal muscle because of its importance in maintaining metabolic control and mobility with age, but also examined the liver because of the effects of metformin on glucoregulation (Madiraju et al., 2014). Our primary hypothesis was that mitochondrial remodeling to the energetic stress of metformin would differ between HCRs and LCRs. Thus, we hypothesized that metformin would result in positive mitochondrial remodeling in LCRs but would be either inconsequential or potentially detrimental for energetics in HCRs. Finally, we included a metformin washout group to help differentiate the long-term effects of metformin treatment from the acute presence of metformin in the tissue. The outcomes of these studies will help delineate for whom metformin may be beneficial and for whom it may be counterproductive.

## 2 | RESULTS

### 2.1 | Metformin dosing was similar among groups

HCR and LCR male rats were singly housed and randomly assigned to a CON group, an MET group, or an MET group with a 48-h washout of metformin prior to euthanasia (MET-WO). For the first 7 days, the MET and MET-WO groups received 100 mg/kg/day of metformin in drinking water with noncaloric flavoring (Mio) to improve palatability (Figure 1a). After the first 7 days, we increased the dose to 200 mg/kg/day for the remainder of the study. The MET-WO had metformin removed 48-h prior to euthanasia. Control rats received tap water with noncaloric flavoring. Animal weight was measured weekly and water consumption was monitored daily to adjust metformin concentration in the water to maintain the appropriate dose based on individual weight and water consumption of each animal (Figure S1a,b). As expected, the plasma concentration of metformin was greater in the MET groups compared to the CON and WO, while WO and CON were similar in both HCR and LCR (Figure S1c). These data suggest that the pharmacokinetics or dynamics of metformin does not differ between the HCRs and LCRs.

### 2.2 | Metformin induces a modest but positive effect on body composition in the LCRs with potential detriments to muscle mass in HCR

As expected, LCRs were heavier, had greater fat mass percentage, and lower lean mass percentage than the HCRs (main effect of strain, Figure 1b–d). Metformin affected the body composition of HCRs and LCRs differently. In LCRs, there were overall positive effects of MET where body mass was lower primarily due to a lower fat mass percentage with no differences in muscle masses (Figure S1). In contrast, the lower body mass in HCR-MET compared to HCR-CON appears to be due to loss of muscle mass (recorded in four of the five muscles; Figure 1e–i) with no loss of fat mass. With MET-WO, there were unexpected differences in body composition over such a short period of time. LCR-MET-WO had a greater fat mass percentage compared to the LCR-MET (Figure 1c) and greater lean mass percentage compared to CON (Figure 1d), while the HCR-MET-WO had a greater lean mass percentage compared to CON and MET (Figure 1d). Because of the unexpected differences in body composition from acute MET-WO, we analyzed body water percentages and found that differences in body water percentage tracked with differences in percent lean mass (Figure 1j). We measured gastrocnemius (gastroc) glycogen concentrations to determine if the shifts in body water were from differences in muscle glycogen storage (Figure 1k). There were notable differences in muscle glycogen storage between the stains, and significantly lower glycogen concentrations after MET-WO in the HCR (but not LCR). However, these differences could not explain the changes in the body water pool. One further insight into the potential changes in the body water pool comes from our labeling with deuterium oxide ($D_2O$) (to measure protein synthesis) over the last week of the study. In both strains, the MET-WO had higher body water enrichment than MET (Figure S1n). When consuming $D_2O$-supplemented drinking water, there can be differing resultant body water pool deuterium enrichments between animals because of differences in metabolically produced water. Our data show that potential changes in macronutrient oxidation (potentially greater fat oxidation) during MET-WO impacted the body water pool size, confounding measurements of body composition. We conclude that there were benefits to body composition in LCRs, but potential detriments to muscle mass in HCRs.

### 2.3 | AMPK is elevated in response to the removal of metformin

Previous studies have indicated that the primary mechanism of action of metformin is through CI inhibition or reducing mitochondrial membrane potential (Brunmair et al., 2004; Owen et al., 2000; Wessels et al., 2014). The resultant energetic stress activates AMPK, which initiates a host of downstream effects (Kjøbsted et al., 2018). In HCRs, after 4 weeks of MET, there was no difference in AMPK activation in the gastroc (Figure 2) or liver (Figure S2c) compared to CON. This finding indicates that MET did not activate AMPK in HCRs, or that compensatory changes over the 4 weeks corrected any energetic stress. However, in skeletal muscle (but not liver) of HCRs, 48-h of MET-WO resulted in higher levels of AMPK phosphorylation compared to CON or MET, indicating that the MET-WO created an energetic stress. In LCRs, MET resulted in higher AMPK phospho/total ratios compared to CON, but this was primarily due to lower total AMPK rather than higher phosphorylation. With MET-WO, this difference from CON remained without any further changes from the MET (Figure 2). Although the primary site of the therapeutic benefits of MET are thought to be at

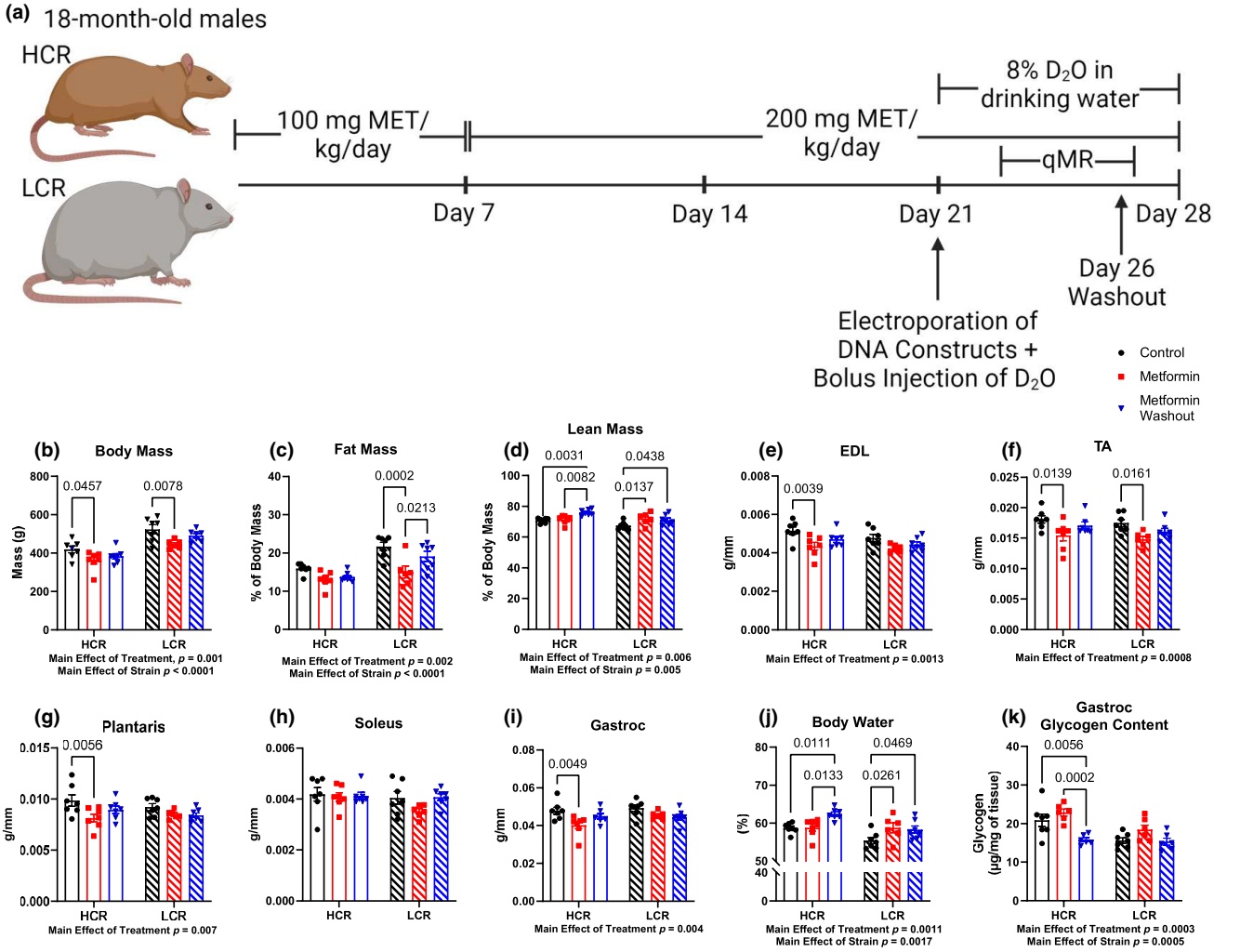


FIGURE 1 (a) Study design. Age-matched, 18-month-old high-capacity runner (HCR) and low-capacity runner (LCR) male rats were randomly assigned to one of three groups: a control group (CON), an acute metformin-treated group (MET), a 48-h washout metformin group (MET-WO). The MET and MET-WO groups received 100 mg/kg/day of metformin in drinking water for the first 7 days of treatment. After day 7, the metformin dose was increased to 200 mg/kg/day. The MET rats received metformin until the day of sacrifice, whereas the MET-WO rats were switched back to tap water 48 h prior to euthanasia. The CON rats received regular tap water. All rats underwent deuterium oxide ($D_2O$) stable isotope labeling during the last week of the intervention. (b–d) Body composition measures from CON (black), MET (red), and MET-WO (blue). (e–i) Skeletal muscle masses normalized to tibial length. (j) Total body water percentage. (k) Gastroc glycogen content. Data were analyzed by two-way ANOVA (group × treatment) and are represented as mean ± SEM from 6 to 7 rats per group.

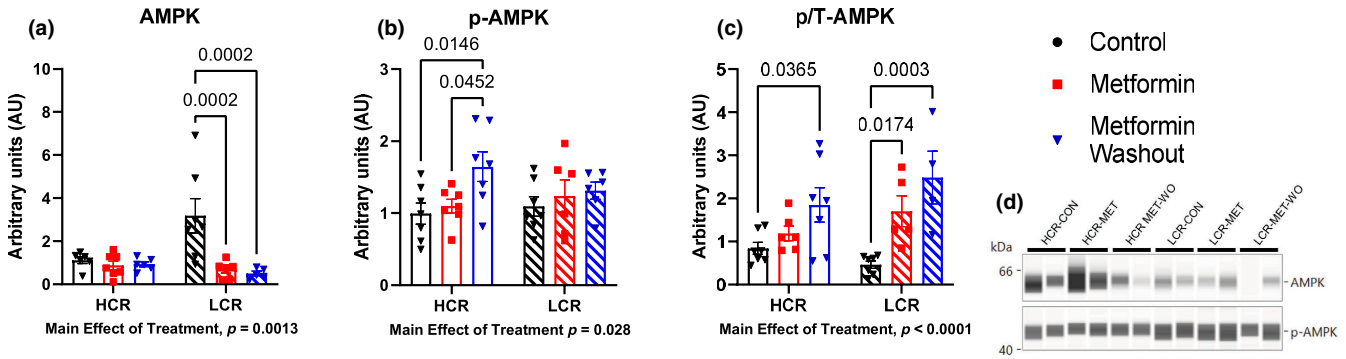


FIGURE 2 Determination of the nutrient sensing marker AMPK, (a) total, b, phosphorylated (Thr172), and c, phospho:total ratio in the gastroc. Data were analyzed by two-way ANOVA (group × treatment) and are represented as mean ± SEM from 6 to 7 rats per group.

the liver, we found minimal evidence that MET differentially impacted HCRs and LCRs at the liver. Our results show that Liver PEPCK mRNA expression was lower in HCR-MET compared to CON but show no differences in liver mass, triglycerides, AMPK, S6 or transcription of the gluconeogenic enzymes G6Pase (Figure S2).

## 2.4 | HCRs and LCRs have heterogenous mitochondrial remodeling in response to 28 days of metformin

Protein remodeling is a primary cellular mechanism of stress adaptation. Protein synthesis is the most energetically costly cellular process (Rolfe & Brown, 1997), which can be compromised during periods of energetic stress. We therefore performed a series of analyses to determine if MET impaired protein remodeling in skeletal muscle, and if the adaptations of mitochondrial proteins to MET differed between the strains. By providing $D_2O$ in drinking water over the final week of treatment, we measured the cumulative protein synthesis over that period when a new steady state was assumed to be achieved. As a general indicator of whether a potential energetic stress from MET compromised protein turnover, we investigated bulk protein turnover in the gastroc, soleus, and tibialis anterior (TA) (Figure 3) and liver (Figure S2g,h). There were no differences in bulk protein turnover of any tissue protein fraction with MET indicating that protein turnover was not compromised.

Mitochondria are one of the primary targets of metformin (Brunmair et al., 2004; Owen et al., 2000; Wessels et al., 2014). Therefore, we used a targeted proteomic analysis to examine changes to protein concentrations of individual proteins in the ETS of gastroc and soleus (Miller, Reid, et al., 2020). We used the gastroc and soleus due to their different fiber type compositions and mitochondrial content. Our targeted panel consisted of 62 proteins; 28 from CI, three from Complex II (CII), 12 from Complex III (CIII), eight from Complex IV (CIV), and 11 from Complex V (CV) (details of validation are provided Table S1). We present our data as dot plots to visualize concentrations relative to each other (Figure 4a,b) and with 3D visualization to determine if there was a spatial relationship (e.g., within or between complexes) of any changes in concentration (Figures S3 and S4; video representations are available at DIO: 10.6084/m9.figshare.25301230). In the gastroc and soleus, there was a main effect of strain where HCRs had greater concentration of ETS proteins compared to LCRs (Figure 4a,b, respectively). After 4 weeks of MET in HCRs, there were no differences in the concentrations of any ETS proteins in the gastroc when compared to CON (Figure 4a). However, in the soleus, HCR-MET had lower concentrations of 18 (six CI, three CIII, four CIV, and five CV) proteins compared to the CON. Half of the proteins were in the mitochondrial matrix, while the other half were in the mitochondrial membrane (Figure S4), suggesting no spatial relationship. In contrast to HCRs, MET did not change mitochondrial protein concentrations in either gastroc or soleus of LCRs (Figure 4a,b and Figures S4 and S5). The measurement of proteins concentrations provides insight into net changes, but not dynamic remodeling since protein turnover can increase without changes in concentration.

To determine the dynamic remodeling of the mitochondrial proteome, we further analyzed the proteomic data for the synthesis rates of the individual proteins by the incorporation of $D_2O$. By applying the three-dimensional modeling, we observed that in general, proteins in the mitochondrial membrane for CI and CV (but not CII, CIII, or CIV) turnover at a slower rate compared to those outside of the mitochondrial membrane (Figure 4c,d and Tables S2 and S3), which has been previously observed (Karunadharma et al., 2015). In the gastroc of the HCRs, MET had slower mitochondrial protein synthesis rates for CI (despite no changes in concentration) compared to CON, whereas other complexes were largely unaffected (Figure 4c and Table S2). In the soleus of HCRs, 11 proteins changed synthesis rates (6 proteins had higher synthesis rates: two CI, one CIII, one CIV, and two CV and 5, while five proteins had lower synthesis rates: three CI, two CIII, and one CIV) in MET compared to CON (Figure 4d and Table S3). In the soleus of the LCRs, MET resulted in 13 CI proteins having greater synthesis rates, of which four proteins are core subunits, and one protein had a slower synthesis rate compared to CON. Also, in LCRs, seven of 10 CV proteins (6/7 proteins were in the matrix) had greater synthesis rates compared to CONs, while there was little impact on CV in HCRs (Figure 4d and Table S3). Notably, changes in turnover of the mitochondrial proteins did not always match with changes in concentration. Even though bulk mitochondrial protein fractional synthesis rates (FSR) did not change in response to metformin, our quantitative and kinetic proteomics suggest that metformin causes more mitochondrial remodeling in LCRs than HCRs.

## 2.5 | Metformin removal induces rapid mitochondrial remodeling that is distinct in each strain

When we removed metformin, there were surprising changes in abundance and synthesis in that short period of time. We show no differences in mitochondrial FSR in the gastroc (Figure 3a). In HCR-MET-WO, mitochondrial FSRs were greater in the soleus and TA compared to HCR-MET. In LCR-MET-WO, mitochondrial FSRs were greater in the soleus compared to LCR-CON and LCR-MET, with no differences in the TA. Additionally, our quantitative and kinetic proteomics assays show that in the gastroc of the HCRs, where MET had minimal differences in turnover, there were substantial differences in synthesis rates among the complexes (Figure 4c). In HCR-MET-WO, most of the proteins were greater than MET (similar to CON), whereas a few proteins were greater than the CON, suggesting a rebound in synthesis rates after the WO. In the gastroc of LCRs, MET resulted in greater synthesis rates compared to CON, while the MET-WO resulted in greater synthesis rates compared to MET and CON (Figure 4c and Table S2). These changes in synthesis rates resulted in minor changes in mitochondrial protein concentrations (Figure 4a). In contrast to the gastroc, the changes in synthesis rates

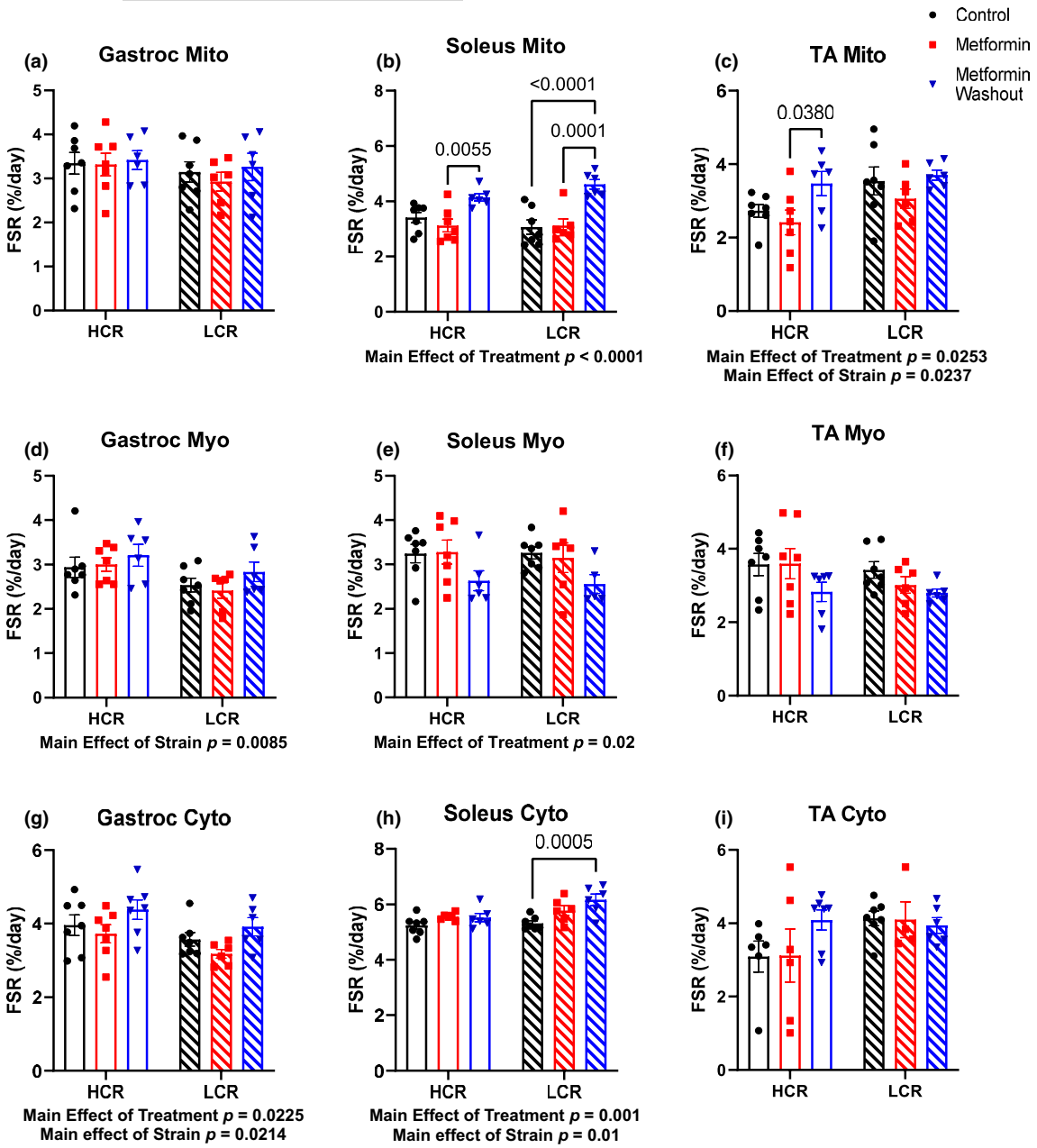


FIGURE 3 Determination of the fractional synthesis rates in (a–c), mitochondrial (Mito), (d–f), myofibrillar (Myo) fractions, and (g–i) cytosolic (Cyto) of the gastrocnemius (gastroc), soleus, and tibialis anterior (TA) muscles. Data were analyzed by two-way ANOVA (group × treatment) and are represented as mean ± SEM from 4 to 7 rats per group.

of the individual mitochondrial proteins from the MET-WO resulted in changes in protein concentrations in the soleus (Figure 4b,d and Table S3). These changes in synthesis and concentration were evident in both strains, although the impacted proteins were not always the same between the strains (Figure 4d and Table S3). In the case of the LCRs, the MET-WO made the mitochondrial proteome concentrations similar to HCR-CON (Figure 4b). It is worth reiterating our labeling approach to grasp the magnitude of the changes in synthesis over the short MET-WO period. Our labeling approach measures cumulative synthesis of proteins over the last week. The MET-WO was only the last 48-h of that 1-week period, so the degree of the changes apparent with MET-WO are above the similar amount of synthesis that would have occurred in MET and MET-WO groups up to that point. Last, it is important to note that there were exceptions to these patterns within the MET-WO of both strains, suggesting some level of heterogeneity in the response to MET-WO between strains.

## 2.6 | Removal of metformin induces mitochondrial fission in the subsarcolemmal population

The second primary mechanism of mitochondrial remodeling are fission–fusion events that change mitochondrial morphology

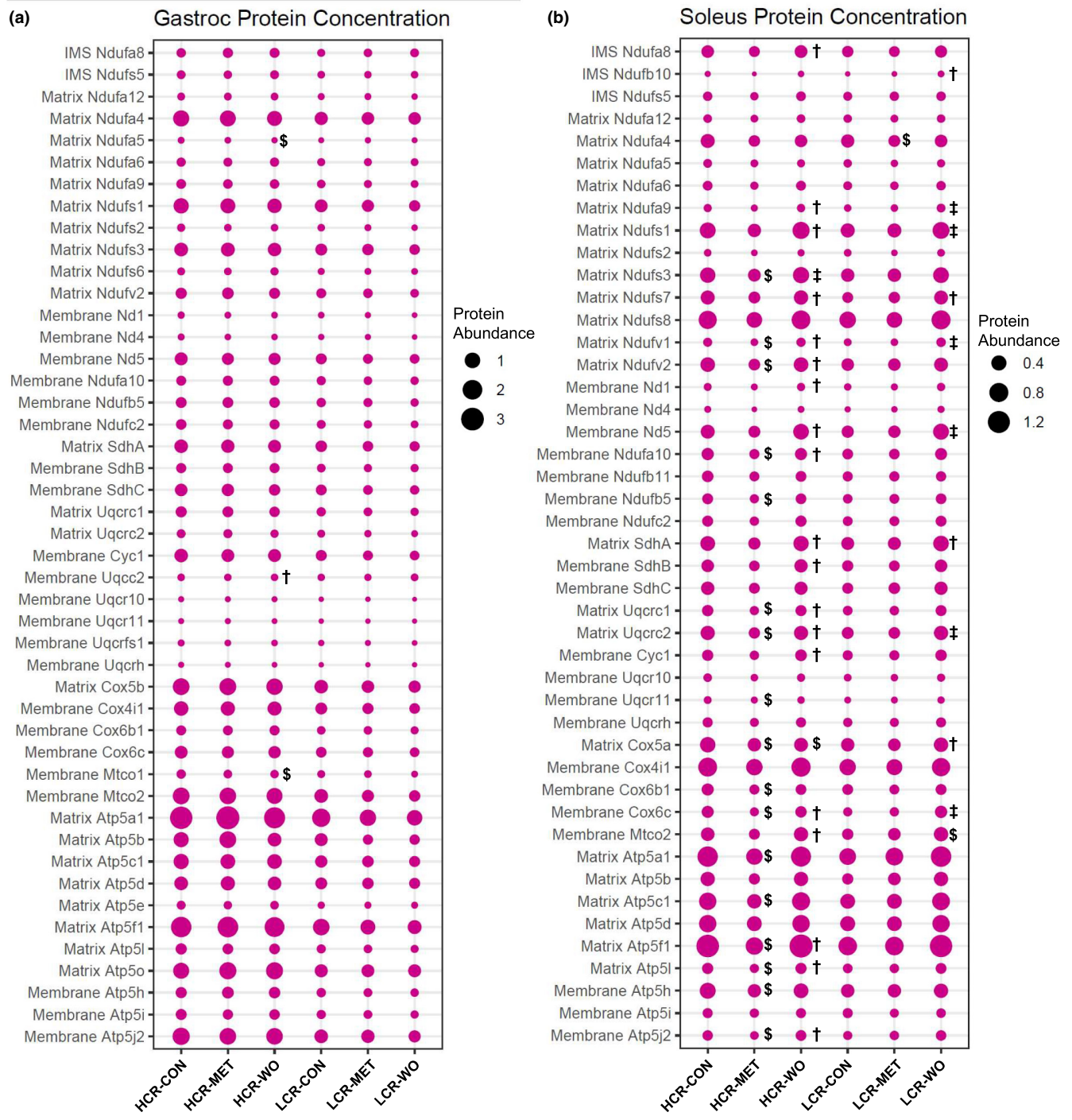


FIGURE 4 We performed a mitochondrial targeted quantitative proteomics in rat gastroc and soleus skeletal muscles. The size of the dot indicates the relative abundance of the protein in the (a) gastroc and (b) solues. Visualization of the synthesis rates (K[1/day]) of the mitochondrial electron transport system complexes (CI, CII, CIII, CIV, CV) in the (c) gastroc and (d) soleus. Blue indicates a faster synthesis rate, whereas red indicates a slower synthesis rate. Gray proteins indicate that the protein was not detected in our analyses. The complexes were generated using complex IDs (CI: 7AK5, CII: 1ZOY, CIII: 7TZ6, CIV: 7COH, and CV: 8H9V) from the RCSB Protein Data Bank and rendered using ChimeraX. Data were analyzed by two-way ANOVA (group × treatment) and are represented as mean from 5 to 7 rats per group. Within each strain $ indicates a significant difference from control group (CON), † indicates a significant difference from metformin-treated (MET) group, and ‡ indicates significant differences from CON and MET.

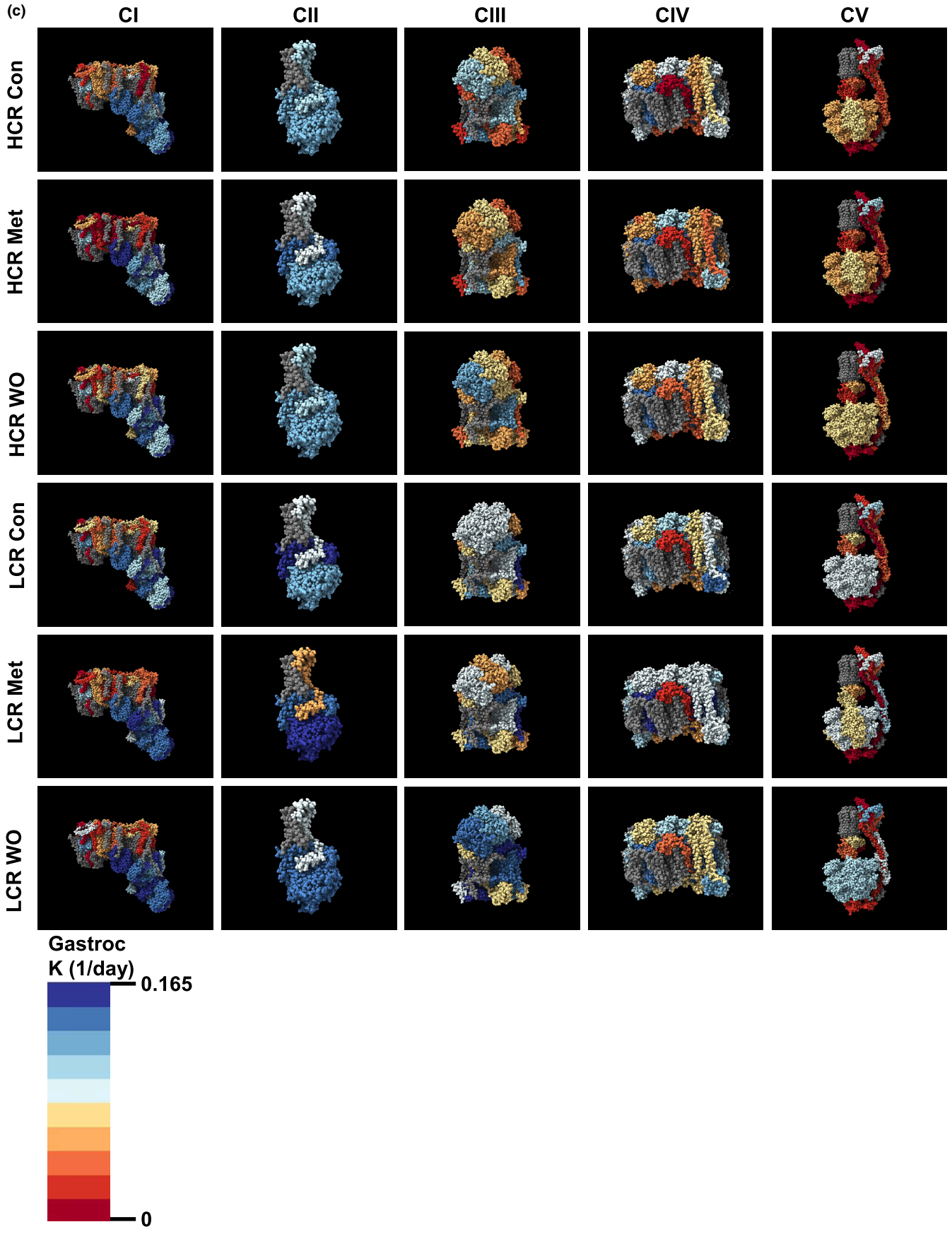


FIGURE 4 (Continued)

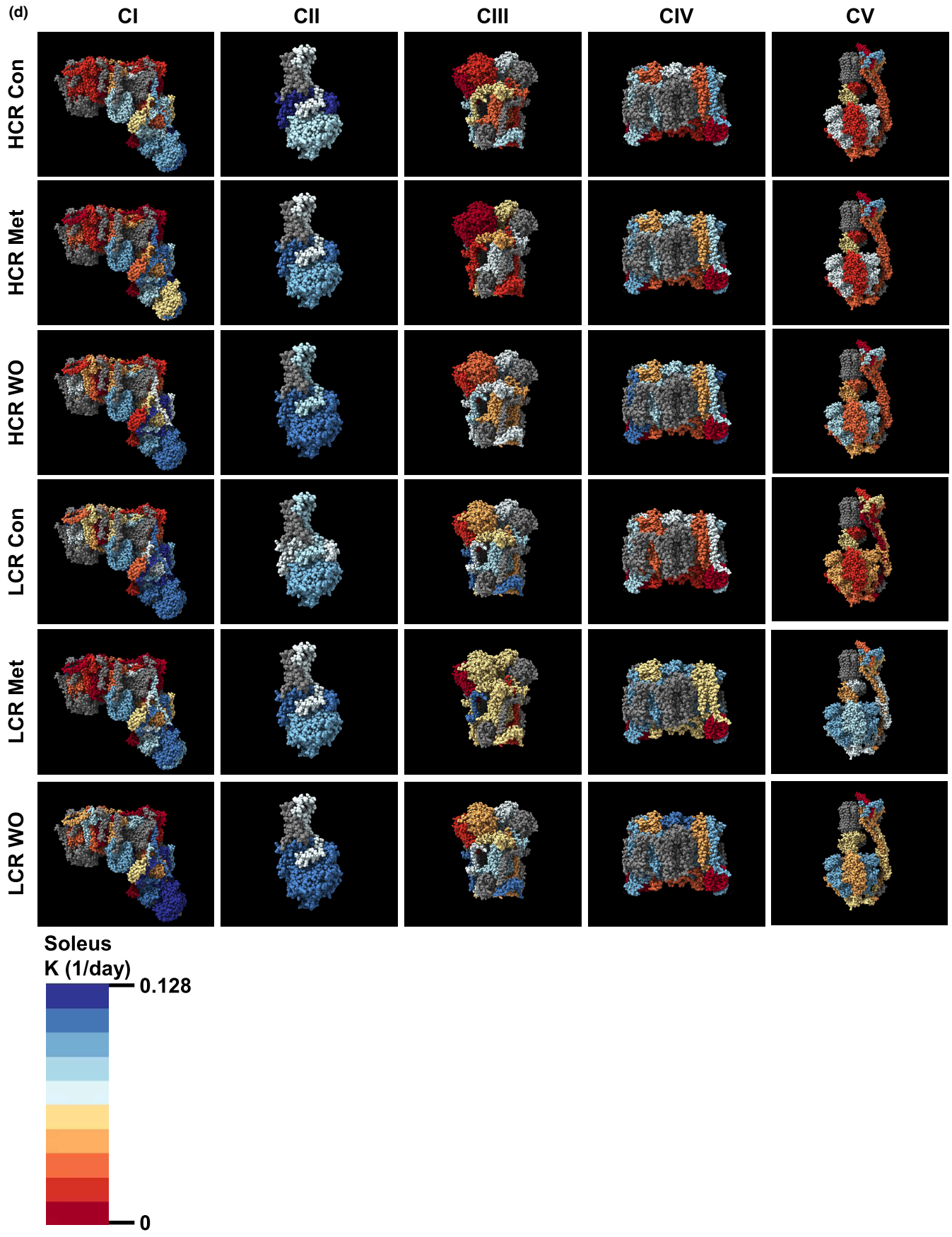


FIGURE 4 (Continued)

(Westrate et al., 2014). We first performed western blotting on protein markers of fission and fusion in the TA. Although there was a main effect of strain on MFF, MFN2, and OPA1 (Figure 5a,d,e), there were no differences within a strain from MET or MET-WO (Figure 5a–e). Given the limited insight provided by these snapshots, we examined changes in mitochondrial morphology. To do so, we electroporated the TA with constructs to label mitochondria with mitochondria-targeted fluorescent reporters. We used TA due to its relative ease for electroporation. Skeletal muscle mitochondria reside in two spatially distinct subpopulations: subsarcolemmal mitochondria (SS) found along the cell perimeter and interfibrillar mitochondria located between the myofibrils. These populations are functionally distinct and respond to stimuli differently (Ferreira et al., 2010; Palmer et al., 1977). To our knowledge, there is no data on the effects of metformin on these mitochondrial populations in skeletal muscle. For our analyses, SS were defined as the mitochondria located in the outer 10% of the cross section of the fiber. MET did not change mitochondrial morphology in HCRs (Figure 5f–n) but resulted in a higher ratio of mitochondrial CSA to muscle fiber CSA in LCRs (Figure 5k). However, 48-h of MET-WO caused differences in the distribution of mitochondria in both strains that were largely driven by decreased SS area (Figure 5g). In both strains, compared to MET, MET-WO had lower SS area (Figure 5g) and SS CSA/total mitochondrial CSA (Figure 5i), suggesting that the MET-WO induces rapid changes to the SS population. These results were somewhat expected as the SS population responds more rapidly to stimuli and are less spatially restricted than IMF (Chomentowski et al., 2011; Ferreira et al., 2010). When expressed relative to muscle fiber CSA, IMF CSA was higher after MET-WO in HCRs, but lower in LCRs (Figure 5m). In sum, by 4 weeks of MET, the mitochondrial pool was expanded relative to fiber CSA in LCRs with undetectable changes in HCRs. However, MET-WO resulted in a rapid alteration in morphology to favor greater IMF relative to muscle CSA in HCRs but lower IMF in LCRs. Our results clearly demonstrate differences in

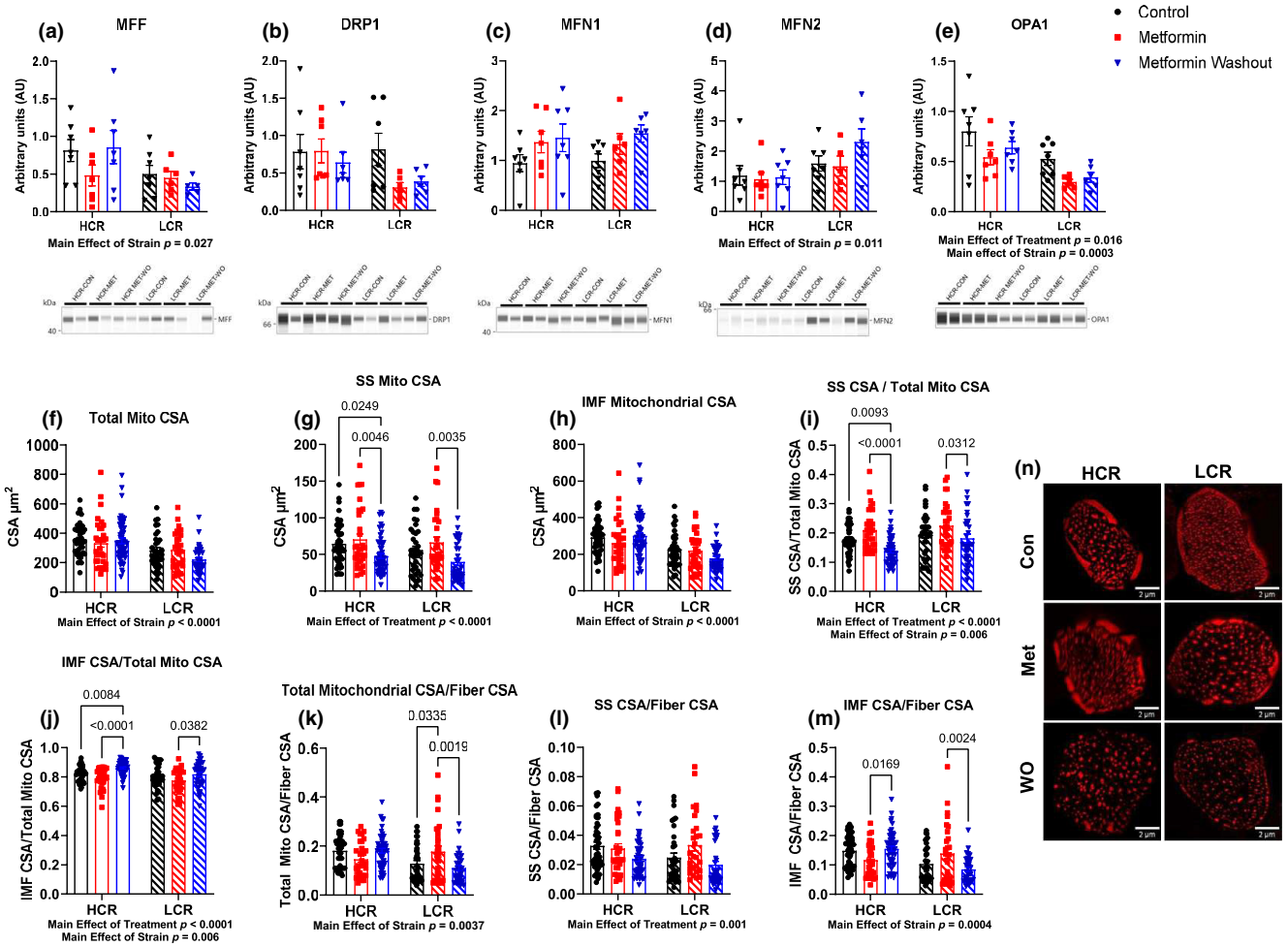


FIGURE 5 (a–e) Mitochondrial dynamics markers. The average cross-sectional area (CSA) of the (f) total mitochondria, (g) subsarcolemmal population, and (h) intermyofibrillar population. (i) The total subsarcolemmal CSA normalized to total mitochondrial CSA. (j) The total intermyofibrillar CSA normalized to total mitochondrial CSA. (k) The total mitochondrial CSA normalized to total fiber CSA. (l) The total subsarcolemmal CSA normalized to total fiber CSA. (m) The total intermyofibrillar CSA normalized to total fiber CSA. (n) Representative images showing the tom20tdtomato channel. Data were analyzed by two-way ANOVA (group × treatment) and are represented as mean ± SEM from 3 to 7 fibers taken from a single image from 6 to 7 rats per group.

the number, size, and percentage of SS in HCRs versus LCRs TA muscle fibers, and that metformin impact these mitochondrial populations differently.

## 2.7 | Metformin inhibits mitochondrial respiration, but the washout increases respiration capacity in HCRs

To assess the resultant differences in mitochondrial respiratory function from the remodeling period, we performed high-resolution respirometry on the gastroc. We used our established ADP titration protocol that previously showed that MET inhibited the positive effects of exercise (Konopka et al., 2019). This protocol uses CI substrates and an ADP titration to determine ADP sensitivity (Konopka et al., 2019) and maximal oxygen consumption. After establishing maximal respiration ($V_{max}$), we use succinate to determine maximal CI+II activity, and rotenone to inhibit CI to determine effects downstream of CI.

As expected, there was a main effect of strain where HCRs had a higher $V_{max}$ than LCRs (Figure 6a) demonstrating the difference in intrinsic aerobic capacity between HCR and LCRs. Four weeks of MET impaired respiration at higher ADP concentrations in LCRs and HCRs, although in HCRs this impairment displayed a trend ($p=0.06$, Figure 6b,c). These data show that our proposed dose of metformin, which is equal to clinical doses in humans and the TAME trial (Barzilai et al., 2016), impairs respiration in HCRs and LCRs (up to 40% and 50%, respectively). In rats with a 48-h MET-WO, there was a striking change in respiration that differed by strain. In HCRs, MET-WO increased $O_2$ flux at all concentrations of ADP to a level that exceeded both CON and MET. In LCRs, the respiration rate in MET-WO was greater than LCR-MET but was equal to CON. To test whether potential differences were the result of the presence or absence of MET, we used fiber bundles from the MET-WO groups in a separate instrument and spiked the respiration chamber with MET. The metformin-spike had no impact on $O_2$ flux in LCRs, but slightly impaired respiration in HCRs where $O_2$ flux was still significantly higher than MET, but no longer different than CON. These differences with MET-WO in HCRs persisted when succinate was added to the chamber and when CI was inhibited with rotenone (Figure S5), indicating that the increase in $O_2$ flux during MET-WO was not solely a CI effect. Further, these differences were apparent

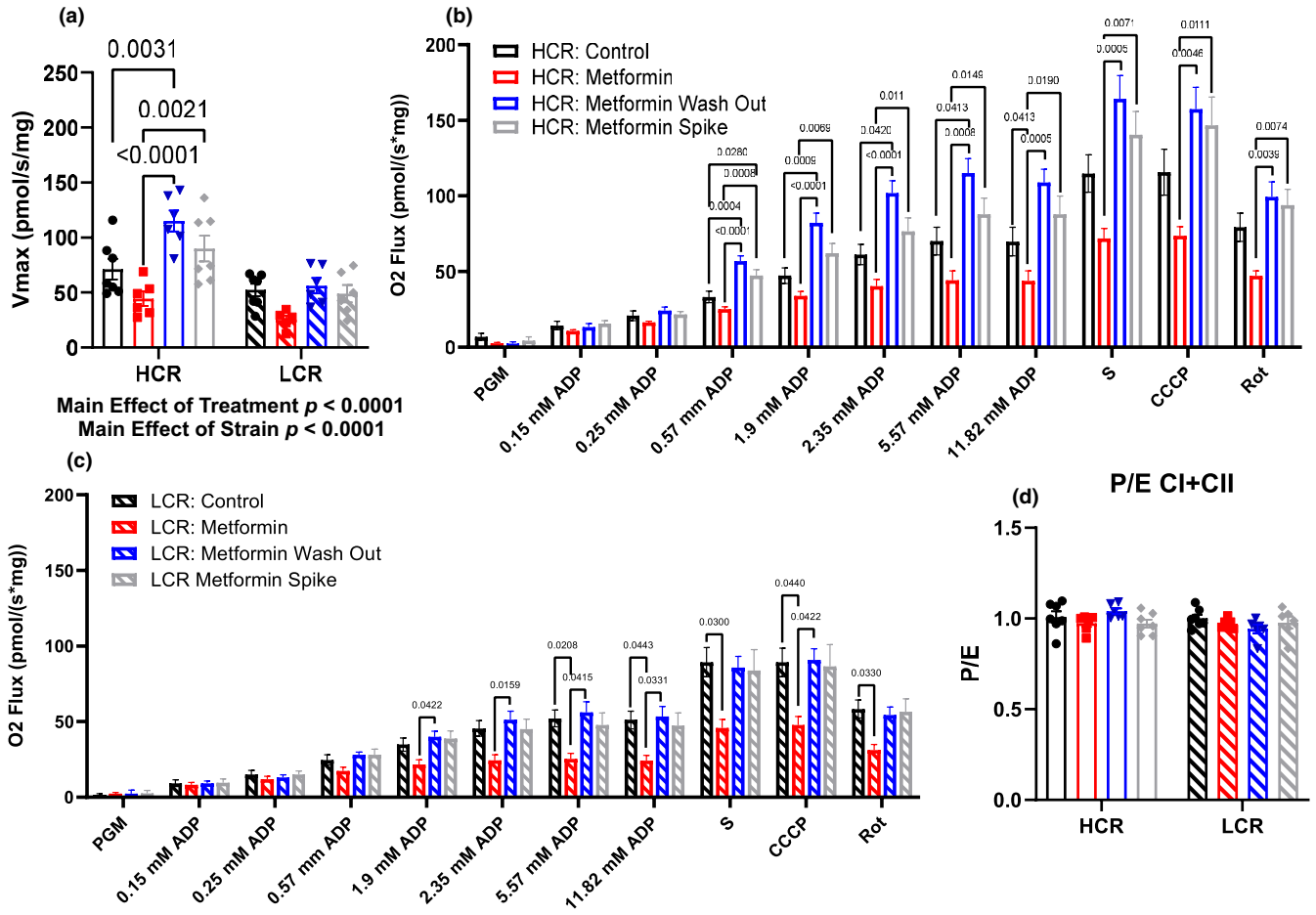


FIGURE 6 (a) Maximal mitochondrial respiration ($V_{max}$). Mitochondrial respiration in (b) HCRs and (c) LCRs. The apparent Km of ADP was calculated using Michaelis–Menten kinetics. Data were analyzed by two-way ANOVA (a and d) or by one-way ANOVA for each substrate addition (b and c) within each strain. Data are represented as mean ± SEM from 4 to 7 rats per group. HCR, high-capacity runner; LCR, low-capacity runner.

when uncoupling. We therefore looked at the oxphos to electron transport capacity ratio (P/E) as an indicator of potential deficiencies in oxphos (Figure 6d). There were no differences in the P/E with any treatment in either strain, indicating that impairments and compensatory changes in mitochondria were due to the effect of MET on electron transfer rather than phosphorylation. In sum, it appears that during metformin treatment, HCRs make better compensatory changes to maintain respiration compared to LCRs. These compensatory changes become apparent in HCRs when metformin is removed, and flux is much greater compared to CON or MET, but in LCRs the changes are not different from CON. Since the MET-Spike changes flux to not be different from CON in HCRs, but does not further impact LCRs, we conclude that the acute presence of MET differentially impacts $O_2$ flux in rats with high or low intrinsic aerobic mitochondrial function (i.e., context specific).

## 3 | DISCUSSION

This study shows complex changes in muscle mitochondrial structure and function with 4 weeks of metformin treatment that rapidly adjusted again upon the removal of metformin. These changes to metformin treatment and its subsequent removal were different depending on intrinsic mitochondrial function (HCRs vs. LCRs), the oxidative capacity of the muscle (gastroc vs. soleus), and the mitochondrial population (IMF vs. SS). Metformin caused lower ADP-stimulated respiration in LCRs, with less of a change in HCRs. However, the washout of metformin resulted in a doubling of respiratory capacity in HCRs, with a more modest increases in LCRs. These improvements in respiratory capacity appear to be caused by mitochondrial remodeling that included increases in protein synthesis and changes in morphology. In line with our hypotheses, the impact of metformin differed by intrinsic mitochondrial function. However, the changes were more complex than anticipated and dependent on whether metformin was acutely present. From this relatively short treatment, there is context specificity to metformin treatment, although how these effects manifest over the long-term remain unclear.

Metformin treatment had positive effects on body composition in the LCRs, with an unexpected loss of muscle mass in HCRs. Prior reports have shown that the quadriceps and soleus muscles of db/db mice decrease in response to metformin treatment while the EDL, gastroc, and TA were unaffected suggesting the glucose-lowering effect of metformin maybe partially offset by loss of muscle mass (Kang et al., 2022). These changes in muscle mass likely have functional consequences. Our results show that the consequences of metformin on skeletal muscle mitochondrial structure and function were strain specific. Our measurements of mitochondrial respiration and morphology were after four-weeks of metformin treatment and mitochondrial protein turnover were cumulative changes over the last week. Therefore, it is hard to say whether the observed remodeling caused changes in mitochondrial respiration or whether changes in mitochondrial respiration triggered the remodeling. However, after metformin treatment the concentration of several mitochondrial proteins was lower in the soleus of HCRs compared to controls. This same decrease was not observed in LCRs and in fact there was a greater mitochondrial CSA. In both strains, the changes in mitochondrial protein concentrations were more prominent in the oxidative soleus compared to the more mixed gastroc. There were changes in synthesis rates of the individual mitochondrial proteins although these differed by strain. Despite these changes, LCR+MET had significantly lower mitochondrial respiration than CON, while the differences in HCR did not reach significance. Metformin-induced inhibition of mitochondrial respiration was not just a complex I phenomenon. This finding agrees with the role of metformin in making the mitochondria more inefficient through changes in membrane potential. We speculate that the changes in mitochondrial protein remodeling are in response to changes in membrane potential. However, this explanation warrants further investigation.

The removal of metformin provided additional insight into how metformin impacts skeletal muscle outcomes under different contexts. After 48-h of metformin washout, cumulative synthesis rates of mitochondrial proteins were greater, with individual proteins driving the effect. These changes were accompanied by increased mitochondrial protein concentrations, and a shift of mitochondrial area from SS to IMF which together presumably drive the robust increase in mitochondrial respiratory capacity. Our interpretation is that the accumulation of metformin in mitochondria caused remodeling to maintain respiratory capacity despite changes in membrane potential. Then, when the metformin was removed, a brake was released, and there was again a remodeling event that transiently strained energetic resources, thus activating AMPK. This mitochondrial remodeling likely transiently strains energetic resources resulting in AMPK activation. An alternative explanation is there was no proceeding remodeling event (or it proceeded very slowly over time) to the onset of metformin treatment, and removing metformin caused rapid remodeling. These findings could explain our previous study where we found that metformin hinders mitochondrial adaptation to exercise (Konopka et al., 2019). It is possible that although the muscle mitochondria can manage to adapt to metformin on board, it cannot further adapt to the addition of an energetic stress. The fission of the SS, as suggested by lower SS CSA relative to total mitochondrial CSA, in response to the washout is likely a contributing factor to the greater mitochondrial respiration capacity in HCRs. The SS turns over at a faster rate and alters oxidative capacity to a greater extent than the IMF in response to changes in energetic demand (Hoppeler et al., 1973; Howald et al., 1985; Kasumov et al., 2013; Krieger et al., 1980). Although we see similar SS mitochondrial morphology in LCRs compared to HCRs, we did not observe any changes in mitochondrial respiration in LCRs after MET-WO. This failure to see the greater mitochondrial respiration in LCR-MET-WO may be due to a shift in cellular priorities. In light of our outcomes, it is possible that the cycling of metformin treatment could be beneficial for long-term healthspan benefits.

There are a few limitations to the current study. First, we did not assess changes that occurred early in response to metformin. There likely were changes in protein synthesis earlier in the treatment phase that we did not capture. Although we were interested in change during

chronic metformin treatment, early changes from metformin would have been interesting to assess from a remodeling perspective. Second, it could be argued that 4 weeks of treatment is not long term; thus, we cannot determine changes in healthspan-related outcomes. We are concerned with the long-term healthspan extension applications of metformin treatment; therefore, our window of application is limited as there is 100% survival at 16 months for both strains, which begins to decline at roughly 18 months for LCRs (Koch et al., 2011). Thus, our metformin treatment begins about at the timepoint when healthspan is in decline. Third, we did not conduct mitochondrial respiration assays in the soleus or TA. The soleus and TA showed large, distinct changes in our proteomic and morphology analyses, respectively. These data could help elucidate the fiber type differences seen with metformin. However, this was not feasible due to the low throughput of high-resolution respirometry. Fourth, these studies were performed in male rats as this was a preliminary study into the effects of metformin in rats with different intrinsic aerobic capacity. Thus, we cannot make conclusions about the context-specific effects of metformin in female rats or between sexes. Fifth, we cannot completely rule out differences in pharmacokinetics or dynamics between HCRs and LCRs, but we would expect that 4 weeks of administration would minimize at least some of these concerns. In addition, a prior study showed no differences in the pharmacokinetics of metformin in healthy subjects and subjects with type II diabetes (Sambol et al., 1996). Future studies should further delineate the timing of changes in oxidative capacity and mitochondrial remodeling to determine causation and add energetic challenges such as exercise to determine limits to remodeling.

In summary, the differences in strains of rats with distinct intrinsic mitochondrial aerobic capacities draw into question whether the positive findings of metformin treatment in human or model organisms that are less metabolically healthy can be broadly applied to all metabolic conditions (Barzilai et al., 2016). We raise this concern because treatments which prolong healthspan would logically start while an individual is healthy and absent of chronic disease (Konopka & Miller, 2019; Miller & Thyfault, 2020). Our current study demonstrates that in skeletal muscle, which is crucial for metabolic health, mobility and mortality, there are clear differences in the effects of metformin based on background metabolic health Additionally, we show that the observed changes from metformin treatment can be dramatically different depending on the acute presence or absence of metformin since there can be (in the appropriate context) rapid mitochondrial remodeling after removal. The findings from this study are critical given the ever expanding off-target use of metformin in healthy individuals without chronic disease and/or overt metabolic dysfunction.

## 4 | MATERIALS AND METHODS

### 4.1 | Ethical approval

We performed all animal procedures in accordance with protocols approved by the Institutional Animal Care and Use Committee at the Oklahoma Medical Research Foundation and the guidelines provided by the National Research Council's Guide for the Care and Use of Laboratory Animals: Eighth Edition.

### 4.2 | Animals

We obtained male, 18-month-old high- and low-capacity runners (HCR/LCR) of the 44th and 45th generation from The University of Toledo. The rats were bred and maintained as previously described (Koch & Britton, 2001). Upon arrival, the rats were randomly assigned to a group and housed individually in a temperature-controlled environment with a 12:12-h light–dark cycle. Throughout the study, rats were given ad libitum access to food (PicoLab Rodent Diet 20, cat #: 3005750-220, 62.4% CHO 24.5% PRO, and 13.1% FAT) and water.

### 4.3 | Experimental design

HCR and LCR male rats were singly housed and randomly assigned to one of three groups: a CON group, an MET group, and a MET group with a 48-h washout of metformin prior to euthanasia (MET-WO). For the first 7 days of treatment, the MET and MET-WO groups received 100 mg/kg/day of metformin in drinking water with noncaloric flavoring (Mio) to improve palatability (Figure 1). After the first 7 days, we increased the dose to 200 mg/kg/day for the remainder of the study. We rationalize that 28 days of metformin was short enough to capture early adaptations to treatment, but long enough to observe potential changes in mitochondrial function. The metformin concentration in the drinking water was based on clinical doses in humans (1500–2000 mg/day). We used allometric scaling with an exponent of 0.75, and our dose was adjusted for the published absolute oral bioavailability (*F*-value) of 29.9% for rats (Choi et al., 2006) versus 33%–55% for humans (Graham et al., 2011). The MET-WO had metformin removed 48 h prior to sacrifice. Control rats received regular tap water with noncaloric flavoring throughout the experiment. Animal weight was measured weekly, and water consumption was monitored daily throughout the treatment to adjust metformin concentration in water to maintain the appropriate dose based on the individual weight and water consumption of each animal. We opted to deliver metformin in the drinking water to better match prior studies (Alfaras et al., 2017) and to avoid the stress of multiple, daily intraperitoneal injections. Additionally, prior literature shows that metformin given in single or multiple doses results in similar average plasma levels of metformin (Graham et al., 2011).

On day 21, all rats received an intraperitoneal bolus injection of filtered 99% $D_2O$ (Sigma Aldrich, St. Louis, MO) equivalent to 5% of body water (estimated at 60% of body mass), followed by 8% $D_2O$-enriched drinking water for the remaining 7 days. Additionally, on day 21, we electroporated one TA with constructs to visualize the outer mitochondrial membrane and matrix. Body composition was measured using quantitative magnetic resonance (QMR, Echo Medical Systems, TX, USA) during the terminal 5 days. Food was removed 12 h prior to sacrifice. Blood from cardiac puncture was

collected into EDTA-lined tubes on ice, and plasma was frozen. The gastro, soleus, and one TA were removed, weighed, flash frozen, and stored at −80°C unless otherwise noted. One TA was fixed in 4% paraformaldehyde and cryo-embedded for mitochondrial morphology analyses.

### 4.4 | Glycogen assay

We quantified glycogen content of the gastrocnemius (gastroc) according to previously established protocols (Schaubroeck et al., 2022) using 20 mg of skeletal muscle powered in liquid nitrogen using 20 mg of skeletal muscle powered in liquid nitrogen. Approximately 20 mg of skeletal muscle was powered in liquid nitrogen and immediately placed in 200 μL of 0.5 M NaOH, which was then placed in a 100°C heating bath for 30 min. Then 50 μL of sodium sulfate and 600 μL of ethanol was added to each solution and centrifuged at 2000 RCF for 10 min. The resulting pellet and glycogen standards were resuspended in 500 μL of DI water and 300 μL of 95% sulfuric acid was quickly added followed by 45 μL of the 5% (w/v) phenol solution. The samples and standers were incubated for 30 min at room temperature. Last, 280 μL of reaction mixture to a microplate, and read in the plate reader at 488 nm in duplicate.

### 4.5 | Semiquantitative immunoblots

For all skeletal muscle data, approximately 20–30 mg of gastroc and TA muscles was lysed and the protein concentration was determined by Peirce 660 assay (cat#: 22660, ThermoFischer Scientific, Waltham, MA) as described previously (Lawrence et al., 2020). Lysed protein fractions were processed to visualize proteins by the ProteinSimple (San Jose, CA, USA) WES system. For primary antibodies, we used AMPK (1:50, #2603), p-AMPK (Thr172) (1:25, #2535 s), Mitofusin-1 (1:50, #14739), Mitofusin-2 (1:50, #11925), MFF (1:50, #84580), DRP1 (1:50, #8570), OPA1 (1:50, #80471), and Tom20 (1:50, #42406 from Cell Signaling). Secondary antibodies were included in a WES Master Kit (DM-001, ProteinSimple). Data were normalized to HCR-CON. Compass files can be found at DIO: 10.6084/m9.figshare.25301230.

For liver analysis, tissue was homogenized in Cell Lysis Buffer (Cat#9806S, Cell Signaling) with protease and phosphatase inhibitors (Cat#5872S, Cell Signaling). We quantified total protein using BCA Protein Assay Regent Kit (cat#23227, Pierce, Rockford, IL, USA). Then we separated proteins into 4%–15% gradient SDS-PAGE gels and transferred them to PVDF immunoblot membranes (Bio-Rad, Hercules, CA). The primary antibodies S6 (1:1000, #2217S), p-S6 (Ser235/236) (1:1000, #2211S), AMPK (1:1000, #2532S), and p-AMPK (Thr172) (1:1000, #2535S, Cell Signaling) were used according to manufacture instructions and IRDye 800CW Infrared secondary antibody (Cat #926-32213, LI-COR Biotechnology, Lincoln, NE) was used at a concentration of 1:15,000. Imaging was done on an Odyssey Fc Imaging System (LI-COR Biotechnology).

### 4.6 | Liver triglycerides

We homogenized 100 mg of liver in Cell Signaling Lysis Buffer (Cat#9806S, Cell Signaling, Danvers, MA) with phosphatase and protease inhibitors (Cat#5872S, Cell Signaling). Total lipid was extracted from this homogenate using the Folch method with a 2:1 chloroform–methanol mixture as previously described (Folch et al., 1957). A nitrogen drier at room temperature was used to dry the lipids prior to reconstitution in 100 μL of 3:1:1 tert-butyl alcohol-methanol-Triton X-100 solution. Triglyceride concentrations were determined using a spectrophotometric assay with a 4:1 Free Glycerol Agent/Triglyceride Agent solution (Cat#: F6428 & T2449, Sigma, Free-Glycerol reagents and Triglyceride, St. Louis, MO) as previously described (Stout et al., 2017).

### 4.7 | Real-time qPCR

We extracted total RNA from liver using Trizol (Life Technologies, Carlsbad, CA), which was reverse transcribed to cDNA with the M-MLV Reverse Transcriptase kit (Life Technologies). We performed RT-qPCR in a 7500 Fast real-time PCR system (Applied Biosystems, Foster City, CA) using TaqMan Fast Universal PCR Master Mix (Life Technologies) and predesigned probes and primers for G6Pase and PEPCK from Applied Biosystems. Target gene expression was expressed as $2^{-\Delta\Delta CT}$ by the comparative CT method (Livak & Schmittgen, 2001) and normalized to the expression of TATA-binding protein (Integrated DNA Technologies).

### 4.8 | GC–MS analysis

For analysis of bulk protein synthesis rates, we fractionated tissues according to our previously published procedures (Konopka, Laurin, et al., 2017; Miller et al., 2012, 2013, 2019; Wolff et al., 2020) including mitochondria, cytosolic, and mixed fractions. The gastroc, soleus, TA, and liver tissues (20–30 mg) were homogenized 1:20 in isolation buffer (100 mM KCl, 40 mM Tris HCl, 10 mM Tris base, 5 mM MgCl2, 1 mM EDTA, and 1 mM ATP, pH = 7.5) with phosphatase and protease inhibitors (HALT, ThermoScientific, Rockford, IL, USA) using a bead homogenizer (Next Advance Inc., Averill Park, NY, USA). The subcellular fractions were then isolated via differential centrifugation and the protein pellets were isolated and purified, 250 μL of 1 M NaOH was added, and pellets were incubated for 15 min at 50°C. Proteins were hydrolyzed in 6 N HCl for 24 h at 120°C. To analyze the deuterium enrichment of alanine in the protein fractions we used Gas Chromatography–Mass Spectroscopy (7890A GC-Agilent 5975C MS, Agilent, Santa Clara, CA) (Abbott et al., 2021; Lawrence et al., 2021).

For analysis of plasma metformin concentrations, we used 100 μL of plasma and added 10 μL an internal deuterated standard (D6). We then added 1 mL acetonitrile to all samples. The supernatant was removed and dried under a vacuum at 45°C. We then derivatized all the samples with 40 μL N-Methyl-bis(trifluoroacetamide) (Millipore Sigma, Burlington, MA), incubated them 1 h at 80°C, then transferred the samples to 4°C to quench the reaction. To measure metformin concentration in the plasma, we used a HP5-MS Agilent capillary column (Agilent, Santa Clara, CA) with electron impact ionization.

### 4.9 | Body water enrichment

To determine body water enrichment, 50 μL of plasma and 0%–12% $D_2O$ standards (Sigma, 151882) were placed into the inner well of an o-ring screw cap and inverted on heating block overnight at 80°C. Samples were diluted 1:300 in ddH2O and analyzed on a liquid water isotope analyzer (Los Gatos Research, Los Gatos, CA, USA) against a standard curve prepared with samples having different concentrations of $D_2O$ (0%–12%). The deuterium enrichments of both the protein (product) and the plasma (precursor) were used to calculate fraction new: fraction new $= E_{product}/E_{precursor}$, where the $E_{product}$ is the enrichment ($E$) of protein-bound alanine and $E_{precursor}$ is the calculated maximum alanine enrichment from equilibration of the body water pool with alanine by MIDA.

### 4.10 | LC–MS/MS analysis

We used a combined targeted quantitative and kinetic proteomics as we previously described (Miller, Pharaoh, et al., 2020). This approach analyzed two to five selected and validated peptides per mitochondrial protein in a series of panels that analyze proteins involved in the mitochondrial complexes as well as membrane-specific (inner and outer). The samples were analyzed using high-resolution accurate mass (HRAM) measurements on a ThermoScientific Q-Exactive Plus hybrid quadrupole-orbitrap mass spectrometer at a $m/z$ resolution of 140,000 configured with a splitless capillary column HPLC system (ThermoScientific Ultimate 3000). For protein quantification, the data were processed using Skyline (MacLean et al., 2010). The response for each protein was taken as the geometric mean of the response for the two to five peptides monitored for each protein. Changes in the abundance of the proteins were determined by normalization to the BSA internal standard. For analysis for kinetic proteomics, we used the $D_2O$me software package (Sadygov et al., 2018), which analyzes the deuterium dependent change in the isotope pattern of each peptide in the full scan MS1 data. A database of mass, retention time, and sequence for each peptide of interest was assembled from LC–MS/MS peptide sequencing experiments on the same tissues. Mass spectral accuracy was confirmed by a <10% deviation from theory using peptides from the BSA internal standard (Mathis et al., 2017).

### 4.11 | Electroporation of DNA construct

To perform imaging of mitochondrial structure, we electroporated the TA 7 days prior to euthanasia with constructs to visualize the outer mitochondrial membrane and matrix. First, legs were shaved using clippers and Nair hair removal. While the rats were under isoflurane, we used an insulin syringe to inject 200 μL of 0.45 U/mL hyaluronidase (Sigma-Aldrich, St. Louis, MO, USA, #:H4272) into the TA muscle belly via three injections (from the distal, lateral, and proximal ends). Two hours after hyaluronidase injection, the rats were again briefly placed on isoflurane and were injected with a total of 20 μg of DNA, 10 μg pCAG-mtYFP (Lewis et al., 2018) and 10 μg of pCAG-TOM20tdTomato via three injections as described above. To electroporate the skeletal muscle, a small amount of Ultrasound Transmission Gel (Aquasonic 100) was placed on the TA. The Tweezertrodes were placed around the TA muscle where one side was located on top of the belly and the other was on the medial head of the gastrocnemius (gastroc). An electrical stimulus was applied with a ECM830 electroporator (model# 45–0662, BTX, Holliston, MA, USA) at a voltage of 86 V, 10 pulses, a pulse length of 20 ms, a distance between electrodes of 2 mm, and 0.5 ms between pulses (Lewis et al., 2018).

### 4.12 | Muscle fixation and sectioning

Immediately following their excision, electroporated TA muscles were placed in 4% paraformaldehyde at 4°C overnight. The following morning, muscles were moved through a 4°C sucrose gradient protocol, starting with 2 h in 10% sucrose in PBS, 2 h in 20% sucrose in PBS, and lastly stored in 30% sucrose in PBS until they were further processed. Muscles were taken out of the 30% sucrose in PBS, pinned onto a piece of cork, and immediately frozen in freezing-cold isopentane. A ½ cm block was cut out of the frozen muscles and placed on a different piece of cork and embedded in OCT before being rapidly placed in freezing-cold isopentane for a minimum of 30 s. Ten-micron thick muscle cross-sections were made using a Cryostar Cryotome and were mounted on slides. Slides were covered with ProLong™ Gold Antifade Mountant (Invitrogen P36930), a coverslip, and left to dry in a dark box at room temp for 24 h. Slides were stored at −20°C until imaged.

### 4.13 | Imaging

We imaged a minimum of five fibers per muscle using a Zeiss LSM 880 with Airyscan FAST (Zeiss, Germany). Randomly selected electroporated fibers were imaged with a 40X oil immersion lens. Following the acquisition of images, the Zeiss ZEN Black program automatically processed the images. Composite images were semi-automatically analyzed using Fiji. We measured fiber cross-sectional area, the number of mitochondrial branches, and mitochondrial cross-sectional area. Additionally, we assessed the co-localization of the two fluorophores used to stain the

mitochondrial outer membrane and the matrix as a proxy of cristae structure. Last, we further analyzed mitochondrial morphology using the same techniques by assessing the two unique mitochondrial populations in skeletal muscle, the intermyofibrillar and the subsarcolemmal, which we defined as the mitochondria located in the outer 10% of the fiber's cross-section. Individual fibers were identified and measured using the polygon tool for fiber cross-sectional area. Each fiber was automatically split by channel (red/green), segmented into four sections, and the brightness/contrast was automatically adjusted for uniformity and then fused back together. The threshold tool was automatically applied to both image channels and particle analysis was performed to assess mitochondrial number and cross-sectional area. The scaling interface identified the outer 10% of the fiber, and the same process was repeated to assess mitochondrial number, and mitochondrial cross-sectional area of the subsarcolemmal mitochondria (Katti et al., 2022).

### 4.14 | High-resolution respirometry

To measure mitochondrial respiration and reactive oxygen species (ROS) production, we used our previously established high-resolution respirometry protocols (Oxygraph-2k, Oroboros Instruments, Innsbruck, Austria) on fiber bundles isolated from the middle third of the lateral head of the gastroc muscle (Groennebaek et al., 2018; Konopka, Castor, et al., 2017; Miller et al., 2017). For our protocol, Glutamate (10 mM), Malate (2 mM), and Pyruvate (5 mM) were added to determine the respiration and ROS production of CI. We then titrated ADP levels (0.125–11.8125 mM) to determine submaximal and maximal CI respiration. We added cytochrome C (10 μm) to determine membrane integrity, followed by Succinate (10 mM) to determine CI + CII respiration (i.e., maximal oxidative phosphorylation) and ROS production. Maximal respiration was determined by uncoupling electron transfer capacity via the addition of the CCCP (1.5 μm) H+ ionophore. The addition of Rotenone (0.5 μm), a CI inhibitor, determined the respiration and ROS production of CII. To determine the acute effects of metformin on mitochondrial respiration, we spiked an Oxygraph-2k chamber with 7.5 μm of metformin, waited 15 min, and then repeated our mitochondrial respiration protocol on another fiber bundle from the MET-WO group.

### 4.15 | Statistical analyses

We performed a two-way ANOVA (strain × treatment) using Graphpad Prism 10 (San Diego, CA, USA) to determine differences between groups and a Tukey post hoc analysis to determine where significant differences occurred unless otherwise stated. For water consumption, we used a two-way repeated measures ANOVA (strain × time). For high-resolution respirometry, we performed a one-way ANOVA for each substrate addition and a Tukey post hoc analysis to determine where significant differences occurred. Outliers as determined by Grubbs' test (alpha = 0.05) and removed from analyses. We presented the results as mean ± standard error (SE) unless otherwise stated with $p$ values less than 0.05 considered to be significant unless otherwise specified. To visual spatial representation of our quantitative and kinetic proteomics, we used dot plots and ChimeraX (Pettersen et al., 2021) software to generate figures using R programming language (3.4.0) and "colorbewer" and "ggplot2" packages (Multivariate Data Analysis, n.d.; R Core Team, 2020).

## AUTHOR CONTRIBUTIONS

MPB, AD, SLB, LGK, and BFM contributed to the design of the work; MPB, AD, CLO, SAM, SMD, AKB, and EV collected the data; MPB, AD, CLO, SAM, JK, SMD, AKB, MET, EV, MTK, MBS, TLL, and BFM analyzed the data; MPB and AD drafted the manuscript; AKB, MTK, SLB, LGK, MBS, TLL, and BFM critically revised the manuscript; and MPB, AD, CLO, SAM, JK, SMD, AKB, MET, EV, SLB, LGK, MTK, MBS, TLL, and BFM approved the agreement to be accountable for all aspects of the work.

## ACKNOWLEDGEMENTS

Some images were created with BioRender.com and ChimeraX. Data processing and analysis were supported by the OMRF Center for Biomedical Data Science. We thank Samantha J. McKee at The University of Toledo for expert phenotyping, care, and maintenance of the LCR/HCR rat colony.

## FUNDING INFORMATION

This work was supported by the National Institutes of Health (T32 AG052363 to M.P.B. and A.D.), NIGMS R35GM137921 (T.L.L), NIGMS 5R24GM137786 IDeA National Resource for Quantitative Proteomics (M.T.K), 5P30AG050911 Oklahoma Nathan Shock Center (M.T.K), 5P20GM103447 Oklahoma INBRE (M.T.K). The National Institutes of Health Office of Research Infrastructure Programs Grant funded the LCR-HCR rat model system P40OD-021331 (L.G.K. and S.L.B.).

## CONFLICT OF INTEREST STATEMENT

The authors have no conflict of interests to disclose.

## DATA AVAILABILITY STATEMENT

All the data generated or analyzed during this study are included in the published article and its Supplementary Information and Source Data files and are available from the corresponding author upon reasonable request. Correspondence and requests for materials should be addressed to B.F.M.

## ORCID

*Matthew P. Bubak* https://orcid.org/0000-0003-4953-4671
*Evelina Volovičeva* https://orcid.org/0000-0002-7313-4822
*Tommy L. Lewis Jr* https://orcid.org/0000-0001-7033-7010

## REFERENCES

Abbott, C. B., Lawrence, M. M., Kobak, K. A., Lopes, E. B. P., Peelor, F. F., Donald, E. J., van Remmen, H., Griffin, T. M., & Miller, B. F. (2021). A novel stable isotope approach demonstrates surprising degree of age-related decline in skeletal muscle collagen proteostasis. *Function*, *2*(4), 1–11. https://doi.org/10.1093/function/zqab028

Alfaras, I., Mitchell, S. J., Mora, H., Lugo, D. R., Warren, A., Navas-Enamorado, I., Hoffmann, V., Hine, C., Mitchell, J. R., Le Couteur, D. G., Cogger, V. C., Bernier, M., & de Cabo, R. (2017). Health benefits of late-onset metformin treatment every other week in mice. *NPJ Aging and Mechanisms of Disease*, *3*(1), 16. https://doi.org/10.1038/s41514-017-0018-7

Aon, M. A., Cortassa, S., Juhaszova, M., González-Reyes, J. A., Calvo-Rubio, M., Villalba, J. M., Lachance, A. D., Ziman, B. D., Mitchell, S. J., Murt, K. N., Axsom, J. E. C., Alfaras, I., Britton, S. L., Koch, L. G., de Cabo, R., Lakatta, E. G., & Sollott, S. J. (2021). Mitochondrial health is enhanced in rats with higher vs. lower intrinsic exercise capacity and extended lifespan. *NPJ Aging and Mechanisms of Disease*, *7*(1), 1. https://doi.org/10.1038/s41514-020-00054-3

Bannister, C. A., Holden, S. E., Jenkins-Jones, S., Morgan, C. L., Halcox, J. P., Schernthaner, G., Mukherjee, J., & Currie, C. J. (2014). Can people with type 2 diabetes live longer than those without? A comparison of mortality in people initiated with metformin or sulphonylurea monotherapy and matched, non-diabetic controls. *Diabetes, Obesity and Metabolism*, *16*(11), 1165–1173. https://doi.org/10.1111/DOM.12354

Barzilai, N., Crandall, J. P., Kritchevsky, S. B., & Espeland, M. A. (2016). Metformin as a tool to target aging. *Cell Metabolism*, *23*(6), 1060–1065. https://doi.org/10.1016/j.cmet.2016.05.011

Blair, S. N., Kohl, H. W. I., Paffenbarger, R. S. J., Clark, D. G., Cooper, K. H., & Gibbons, L. W. (1989). Physical fitness and all-cause mortality. *JAMA*, *262*(17), 2395. https://doi.org/10.1001/jama.1989.03430170057028

Brunmair, B., Staniek, K., Gras, F., Scharf, N., Althaym, A., Clara, R., Roden, M., Gnaiger, E., Nohl, H., Waldhäusl, W., & Fürnsinn, C. (2004). Thiazolidinediones, like metformin, inhibit respiratory complex I. *Diabetes*, *53*(4), 1052–1059. https://doi.org/10.2337/diabetes.53.4.1052

Campbell, J. M., Bellman, S. M., Stephenson, M. D., & Lisy, K. (2017). Metformin reduces all-cause mortality and diseases of ageing independent of its effect on diabetes control: A systematic review and meta-analysis. *Ageing Research Reviews*, *40*, 31–44. https://doi.org/10.1016/j.arr.2017.08.003

Chaudhari, K., Reynolds, C. D., & Yang, S.-H. (2020). Metformin and cognition from the perspectives of sex, age, and disease. *GeroScience*, *42*(1), 97–116. https://doi.org/10.1007/s11357-019-00146-3

Choi, Y. H., Kim, S. G., & Lee, M. G. (2006). Dose-independent pharmacokinetics of metformin in rats: Hepatic and gastrointestinal first-pass effects. *Journal of Pharmaceutical Sciences*, *95*(11), 2543–2552. https://doi.org/10.1002/jps.20744

Chomentowski, P., Coen, P. M., Radiková, Z., Goodpaster, B. H., & Toledo, F. G. S. S. (2011). Skeletal muscle mitochondria in insulin resistance: Differences in intermyofibrillar versus subsarcolemmal subpopulations and relationship to metabolic flexibility. *The Journal of Clinical Endocrinology and Metabolism*, *96*(2), 494–503. https://doi.org/10.1210/jc.2010-0822

Ferreira, R., Vitorino, R., Alves, R. M. P., Appell, H. J., Powers, S. K., Duarte, J. A., & Amado, F. (2010). Subsarcolemmal and intermyofibrillar mitochondria proteome differences disclose functional specializations in skeletal muscle. *Proteomics*, *10*(17), 3142–3154. https://doi.org/10.1002/pmic.201000173

Fitzgerald, L. F., Christie, A. D., & Kent, J. A. (2016). Heterogeneous effects of old age on human muscle oxidative capacity in vivo: A systematic review and meta-analysis. *Applied Physiology, Nutrition and Metabolism*, *41*(11), 1137–1145. https://doi.org/10.1139/apnm-2016-0195

Folch, J., Lees, M., & Sloane Stanley, G. H. (1957). A simple method for the isolation and purification of total lipides from animal tissues. *The Journal of Biological Chemistry*, *226*(1), 497–509. https://doi.org/10.1016/s0021-9258(18)64849-5

Graham, G. G., Punt, J., Arora, M., Day, R. O., Doogue, M. P., Duong, J. K., Furlong, T. J., Greenfield, J. R., Greenup, L. C., Kirkpatrick, C. M., Ray, J. E., Timmins, P., & Williams, K. M. (2011). Clinical pharmacokinetics of metformin. *Clinical Pharmacokinetics*, *50*(2), 81–98. https://doi.org/10.2165/11534750-000000000-00000

Griffin, S. J., Leaver, J. K., & Irving, G. J. (2017). Impact of metformin on cardiovascular disease: A meta-analysis of randomised trials among people with type 2 diabetes. *Diabetologia*, *60*(9), 1620–1629. https://doi.org/10.1007/s00125-017-4337-9

Groennebaek, T., Jespersen, N. R., Jakobsgaard, J. E., Sieljacks, P., Wang, J., Rindom, E., Musci, R. v., Bøtker, H. E., Hamilton, K. L., Miller, B. F., de Paoli, F. v., & Vissing, K. (2018). Skeletal muscle mitochondrial protein synthesis and respiration increase with low-load blood flow restricted as well as high-load resistance training. *Frontiers in Physiology*, *9*, 1796. https://doi.org/10.3389/fphys.2018.01796

Hoppeler, H., Lüthi, P., Claassen, H., Weibel, E. R., & Howald, H. (1973). The ultrastructure of the normal human skeletal muscle—A morphometric analysis on untrained men, women and well-trained orienteers. *Pflügers Archiv European Journal of Physiology*, *344*(3), 217–232. https://doi.org/10.1007/BF00588462

Howald, H., Hoppeler, H., Claassen, H., Mathieu, O., & Straub, R. (1985). Influences of endurance training on the ultrastructural composition of the different muscle fiber types in humans. *Pflügers Archiv European Journal of Physiology*, *403*(4), 369–376. https://doi.org/10.1007/BF00589248

Iannello, S., Camuto, M., Cavaleri, A., Milazzo, P., Pisano, M. G., Bellomia, D., & Belfiore, F. (2004). Effects of short-term metformin treatment on insulin sensitivity of blood glucose and free fatty acids. *Diabetes, Obesity & Metabolism*, *6*(1), 8–15. https://doi.org/10.1111/j.1463-1326.2004.00306.x

Kaeberlein, M. (2018). How healthy is the healthspan concept? *GeroScience*, *40*(4), 361–364. https://doi.org/10.1007/s11357-018-0036-9

Kang, M. J., Moon, J. W., Lee, J. O., Kim, J. H., Jung, E. J., Kim, S. J., Oh, J. Y., Wu, S. W., Lee, P. R., Park, S. H., & Kim, H. S. (2022). Metformin induces muscle atrophy by transcriptional regulation of myostatin via HDAC6 and FoxO3a. *Journal of Cachexia, Sarcopenia and Muscle*, *13*(1), 605–620. https://doi.org/10.1002/jcsm.12833

Karunadharma, P. P., Basisty, N., Chiao, Y. A., Dai, D. F., Drake, R., Levy, N., Koh, W. J., Emond, M. J., Kruse, S., Marcinek, D., Maccoss, M. J., & Rabinovitch, P. S. (2015). Respiratory chain protein turnover rates in mice are highly heterogeneous but strikingly conserved across tissues, ages, and treatments. *FASEB Journal*, *29*(8), 3582–3592. https://doi.org/10.1096/fj.15-272666

Kasumov, T., Dabkowski, E. R., Chandra Shekar, K., Li, L., Ribeiro, R. F., Walsh, K., Previs, S. F., Sadygov, R. G., Willard, B., Stanley, W. C., & Jr, R. R. (2013). Assessment of cardiac proteome dynamics with heavy water: Slower protein synthesis rates in interfibrillar than subsarcolemmal mitochondria. *American Journal of Physiology-Heart and Circulatory Physiology*, *304*, 1201–1214. https://doi.org/10.1152/ajpheart.00933.2012.-Tradi

Katti, P., Hall, A. S., Parry, H. A., Ajayi, P. T., Kim, Y., Willingham, T. B., Bleck, C. K. E., Wen, H., & Glancy, B. (2022). Mitochondrial network configuration influences sarcomere and myosin filament structure in striated muscles. *Nature Communications*, *13*(1), 1–17. https://doi.org/10.1038/s41467-022-33678-y

Kjøbsted, R., Hingst, J. R., Fentz, J., Foretz, M., Sanz, M., Pehmøller, C., Shum, M., Marette, A., Mounier, R., Treebak, J. T., Wojtaszewski, J. F. P., Viollet, B., & Lantier, L. (2018). AMPK in skeletal muscle

function and metabolism. *The FASEB Journal*, *32*(4), 1741–1777. https://doi.org/10.1096/fj.201700442R

Knowler, W. C., Barrett-Connor, E., Fowler, S. E., Hamman, R. F., Lachin, J. M., Walker, E. A., Nathan, D. M., & Diabetes Prevention Program Research Group. (2002). Reduction in the incidence of type 2 diabetes with lifestyle intervention or metformin. *The New England Journal of Medicine*, *346*(6), 393–403. https://doi.org/10.1056/NEJMoa012512

Koch, L. G., & Britton, S. L. (2001). Artificial selection for intrinsic aerobic endurance running capacity in rats. *Physiological Genomics*, *5*(1), 45–52. https://doi.org/10.1152/physiolgenomics.2001.5.1.45

Koch, L. G., & Britton, S. L. (2018). Theoretical and biological evaluation of the link between low exercise capacity and disease risk. *Cold Spring Harbor Perspectives in Medicine*, *8*(1), a029868. https://doi.org/10.1101/cshperspect.a029868

Koch, L. G., Britton, S. L., & Wisløff, U. (2012). A rat model system to study complex disease risks, fitness, aging, and longevity. *Trends in Cardiovascular Medicine*, *22*(2), 29–34. https://doi.org/10.1016/j.tcm.2012.06.007

Koch, L. G., Kemi, O. J., Qi, N., Leng, S. X., Bijma, P., Gilligan, L. J., Wilkinson, J. E., Wisløff, H., Høydal, M. A., Rolim, N., Abadir, P. M., van Grevenhof, E. M., Smith, G. L., Burant, C. F., Ellingsen, O., Britton, S. L., & Wisløff, U. (2011). Intrinsic aerobic capacity sets a divide for aging and longevity. *Circulation Research*, *109*(10), 1162–1172. https://doi.org/10.1161/CIRCRESAHA.111.253807

Konopka, A. R., Castor, W. M., Wolff, C. A., Musci, R. v., Reid, J. J., Laurin, J. L., Valenti, Z. J., Hamilton, K. L., & Miller, B. F. (2017). Skeletal muscle mitochondrial protein synthesis and respiration in response to the energetic stress of an ultra-endurance race. *Journal of Applied Physiology*, *123*(6), 1516–1524. http://www.jappl.org

Konopka, A. R., Laurin, J. L., Musci, R. V., Wolff, C. A., Reid, J. J., Biela, L. M., Zhang, Q., Peelor, F. F., Melby, C. L., Hamilton, K. L., & Miller, B. F. (2017). Influence of Nrf2 activators on subcellular skeletal muscle protein and DNA synthesis rates after 6 weeks of milk protein feeding in older adults. *GeroScience*, *39*(2), 175–186. https://doi.org/10.1007/s11357-017-9968-8

Konopka, A. R., Laurin, J. L., Schoenberg, H. M., Reid, J. J., Castor, W. M., Wolff, C. A., Musci, R. V., Safairad, O. D., Linden, M. A., Biela, L. M., Bailey, S. M., Hamilton, K. L., & Miller, B. F. (2019). Metformin inhibits mitochondrial adaptations to aerobic exercise training in older adults. *Aging Cell*, *18*(1), e12880. https://doi.org/10.1111/acel.12880

Konopka, A. R., & Miller, B. F. (2019). Taming expectations of metformin as a treatment to extend healthspan. *GeroScience*, *41*(2), 101–108. https://doi.org/10.1007/s11357-019-00057-3

Krieger, D. A., Tate, C. A., McMillin-Wood, J., & Booth, F. W. (1980). Populations of rat skeletal muscle mitochondria after exercise and immobilization. *Journal of Applied Physiology: Respiratory, Environmental and Exercise Physiology*, *48*(1), 23–28. https://doi.org/10.1152/jappl.1980.48.1.23

Lawrence, M. M., van Pelt, D. W., Confides, A. L., Hettinger, Z. R., Hunt, E. R., Reid, J. J., Laurin, J. L., Peelor, F. F., Butterfield, T. A., Miller, B. F., & Dupont-Versteegden, E. E. (2021). Muscle from aged rats is resistant to mechanotherapy during atrophy and reloading. *GeroScience*, *43*(1), 65–83. https://doi.org/10.1007/s11357-020-00215-y

Lawrence, M. M., van Pelt, D. W., Confides, A. L., Hunt, E. R., Hettinger, Z. R., Laurin, J. L., Reid, J. J., Peelor, F. F., Butterfield, T. A., Dupont-Versteegden, E. E., & Miller, B. F. (2020). Massage as a mechanotherapy promotes skeletal muscle protein and ribosomal turnover but does not mitigate muscle atrophy during disuse in adult rats. *Acta Physiologica*, *229*(3), e13460. https://doi.org/10.1111/apha.13460

Lewis, T. L., Kwon, S.-K., Lee, A., Shaw, R., & Polleux, F. (2018). MFF-dependent mitochondrial fission regulates presynaptic release and axon branching by limiting axonal mitochondria size. *Nature Communications*, *9*(1), 5008. https://doi.org/10.1038/s41467-018-07416-2

Li, M., Li, X., Zhang, H., & Lu, Y. (2018). Molecular mechanisms of metformin for diabetes and cancer treatment. *Frontiers in Physiology*, *9*, 1–7. https://doi.org/10.3389/fphys.2018.01039

Livak, K. J., & Schmittgen, T. D. (2001). Analysis of relative gene expression data using real-time quantitative PCR and the 2-ΔΔCT method. *Methods*, *25*(4), 402–408. https://doi.org/10.1006/meth.2001.1262

Long, D. E., Peck, B. D., Martz, J. L., Tuggle, S. C., Bush, H. M., McGwin, G., Kern, P. A., Bamman, M. M., & Peterson, C. A. (2017). Metformin to Augment Strength Training Effective Response in Seniors (MASTERS): Study protocol for a randomized controlled trial. *Trials*, *18*(1), 192. https://doi.org/10.1186/s13063-017-1932-5

MacLean, B., Tomazela, D. M., Shulman, N., Chambers, M., Finney, G. L., Frewen, B., Kern, R., Tabb, D. L., Liebler, D. C., & MacCoss, M. J. (2010). Skyline: An open source document editor for creating and analyzing targeted proteomics experiments. *Bioinformatics*, *26*(7), 966–968. https://doi.org/10.1093/bioinformatics/btq054

Madiraju, A. K., Erion, D. M., Rahimi, Y., Zhang, X. M., Braddock, D. T., Albright, R. A., Prigaro, B. J., Wood, J. L., Bhanot, S., MacDonald, M. J., Jurczak, M. J., Camporez, J. P., Lee, H. Y., Cline, G. W., Samuel, V. T., Kibbey, R. G., & Shulman, G. I. (2014). Metformin suppresses gluconeogenesis by inhibiting mitochondrial glycerophosphate dehydrogenase. *Nature*, *510*(7506), 542–546. https://doi.org/10.1038/nature13270

Mathis, A. D., Naylor, B. C., Carson, R. H., Evans, E., Harwell, J., Knecht, J., Hexem, E., Peelor, F. F., Miller, B. F., Hamilton, K. L., Transtrum, M. K., Bikman, B. T., & Price, J. C. (2017). Mechanisms of in vivo ribosome maintenance change in response to nutrient signals. *Molecular & Cellular Proteomics*, *16*(2), 243–254. https://doi.org/10.1074/mcp.M116.063255

Miller, B., Hamilton, K., Boushel, R., Williamson, K., Laner, V., Gnaiger, E., & Davis, M. (2017). Mitochondrial respiration in highly aerobic canines in the non-raced state and after a 1600-km sled dog race. *PLoS One*, *12*(4), e0174874. https://doi.org/10.1371/journal.pone.0174874

Miller, B., Pharaoh, G., Hamilton, K. L., Peelor, F. F., Kirkland, J. L., Freeman, W. M., Mann, S. N., Kinter, M., Price, J. C., & Stout, M. B. (2020). Short-term calorie restriction and 17$\alpha$-estradiol administration elicit divergent effects on proteostatic processes and protein content in metabolically active tissues. *Journals of Gerontology Series A: Biological Sciences and Medical Sciences*, *75*(5), 849–857.

Miller, B. F., Baehr, L. M., Musci, R. V., Reid, J. J., Peelor, F. F., Hamilton, K. L., & Bodine, S. C. (2019). Muscle-specific changes in protein synthesis with aging and reloading after disuse atrophy. *Journal of Cachexia, Sarcopenia and Muscle*, *10*(6), 1195–1209. https://doi.org/10.1002/jcsm.12470

Miller, B. F., Reid, J. J., Price, J. C., Lin, H. J. L., Atherton, P. J., & Smith, K. (2020). CORP: The use of deuterated water for the measurement of protein synthesis. *Journal of Applied Physiology*, *128*(5), 1163–1176. https://doi.org/10.1152/japplphysiol.00855.2019

Miller, B. F., Robinson, M. M., Bruss, M. D., Hellerstein, M., & Hamilton, K. L. (2012). A comprehensive assessment of mitochondrial protein synthesis and cellular proliferation with age and caloric restriction. *Aging Cell*, *11*(1), 150–161. https://doi.org/10.1111/j.1474-9726.2011.00769.x

Miller, B. F., Robinson, M. M., Reuland, D. J., Drake, J. C., Peelor, F. F., Bruss, M. D., Hellerstein, M. K., & Hamilton, K. L. (2013). Calorie restriction does not increase short-term or long-term protein synthesis. *Journals of Gerontology. Series A, Biological Sciences and Medical Sciences*, *68*(5), 530–538. https://doi.org/10.1093/gerona/gls219

Miller, B. F., & Thyfault, J. P. (2020). Exercise-pharmacology interactions: Metformin, statins, and healthspan. *Physiology*, *35*(5), 338–347. https://doi.org/10.1152/physiol.00013.2020

(n.d.). *Multivariate data analysis*. https://scienceinside.shinyapps.io/mvda/

Okita, K., Yonezawa, K., Nishijima, H., Hanada, A., Ohtsubo, M., Kohya, T., Murakami, T., & Kitabatake, A. (1998). Skeletal muscle metabolism limits exercise capacity in patients with chronic heart failure. *Circulation*, *98*(18), 1886–1891. https://doi.org/10.1161/01.CIR.98.18.1886

Owen, M. R., Doran, E., & Halestrap, A. P. (2000). Evidence that metformin exerts its anti-diabetic effects through inhibition of complex 1 of the mitochondrial respiratory chain. *Biochemical Journal*, *348*(3), 607–614. https://doi.org/10.1042/bj3480607

Palmer, J. W., Tandler, B., & Hoppel, C. L. (1977). Biochemical properties of subsarcolemmal and interfibrillar mitochondria isolated from rat cardiac muscle. *Journal of Biological Chemistry*, *252*(23), 8731–8739. https://doi.org/10.1016/s0021-9258(19)75283-1

Pettersen, E., Goddard, T., Huang, C. C., Meng, E. C., Couch, G. S., Croll, T. I., Morris, J. H., & Ferrin, T. E. (2021). UCSF ChimeraX: Structure visualization for researchers, educators, and developers. *Protein Science*, *30*, 70–82.

R Core Team. (2020). *R: A language and environment for statistical computing*. R Foundation for Statistical Computing.

Rasmussen, U. F., Rasmussen, H. N., Krustrup, P., Quistorff, B., Saltin, B., & Bangsbo, J. (2001). Aerobic metabolism of human quadriceps muscle: In vivo data parallel measurements on isolated mitochondria. *American Journal of Physiology. Endocrinology and Metabolism*, *280*(2), E301–E307. https://doi.org/10.1152/ajpendo.2001.280.2.E301

Rolfe, D. F. S., & Brown, G. C. (1997). Cellular energy utilization and molecular origin of standard metabolic rate in mammals. *Physiological Reviews*, *77*(3), 731–758. https://doi.org/10.1152/physrev.1997.77.3.731

Sadygov, R. G., Avva, J., Rahman, M., Lee, K., Ilchenko, S., Kasumov, T., & Borzou, A. (2018). D2ome, software for in vivo protein turnover analysis using heavy water labeling and LC-MS, reveals alterations of hepatic proteome dynamics in a mouse model of NAFLD. *Journal of Proteome Research*, *17*(11), 3740–3748. https://doi.org/10.1021/acs.jproteome.8b00417

Sambol, N. C., Chiang, J., O'Conner, M., Liu, C. Y., Lin, E. T., Goodman, A. M., Benet, L. Z., & Karam, J. H. (1996). Pharmacokinetics and pharmacodynamics of metformin in healthy subjects and patients with noninsulin-dependent diabetes mellitus. *Journal of Clinical Pharmacology*, *36*(11), 1012–1021. https://doi.org/10.1177/009127009603601105

Schaubroeck, K. J., Leitner, B. P., & Perry, R. J. (2022). An optimized method for tissue glycogen quantification. *Physiological Reports*, *10*(4), e15195. https://doi.org/10.14814/phy2.15195

Stevenson-Hoare, J., Leonenko, G., & Escott-Price, V. (2023). Comparison of long-term effects of metformin on longevity between people with type 2 diabetes and matched non-diabetic controls. *BMC Public Health*, *23*(1), 1–6. https://doi.org/10.1186/s12889-023-15764-y

Stout, M. B., Steyn, F. J., Jurczak, M. J., Camporez, J. P. G., Zhu, Y., Hawse, J. R., Jurk, D., Palmer, A. K., Xu, M., Pirtskhalava, T., Evans, G. L., de Souza Santos, R., Frank, A. P., White, T. A., Monroe, D. G., Singh, R. J., Casaclang-Verzosa, G., Miller, J. D., Clegg, D. J., … Kirkland, J. L. (2017). 17*A*-estradiol alleviates age-related metabolic and inflammatory dysfunction in male mice without inducing feminization. *Journals of Gerontology. Series A, Biological Sciences and Medical Sciences*, *72*(1), 3–15. https://doi.org/10.1093/gerona/glv309

Toyama, E. Q., Herzig, S., Courchet, J., Lewis, T. L., Losón, O. C., Hellberg, K., Young, N. P., Chen, H., Polleux, F., Chan, D. C., & Shaw, R. J. (2016). AMP-activated protein kinase mediates mitochondrial fission in response to energy stress. *Science*, *351*(6270), 275–281. https://doi.org/10.1126/science.aab4138

Wang, Y., An, H., Liu, T., Qin, C., Sesaki, H., Guo, S., Radovick, S., Hussain, M., Maheshwari, A., Wondisford, F. E., O'Rourke, B., & He, L. (2019). Metformin improves mitochondrial respiratory activity through activation of AMPK. *Cell Reports*, *29*(6), 1511–1523.e5. https://doi.org/10.1016/j.celrep.2019.09.070

Wessels, B., Ciapaite, J., Van Den Broek, N. M. A., Nicolay, K., & Prompers, J. J. (2014). Metformin impairs mitochondrial function in skeletal muscle of both lean and diabetic rats in a dose-dependent manner. *PLoS One*, *9*(6), e100525. https://doi.org/10.1371/journal.pone.0100525

Westrate, L. M., Drocco, J. A., Martin, K. R., Hlavacek, W. S., & MacKeigan, J. P. (2014). Mitochondrial morphological features are associated with fission and fusion events. *PLoS One*, *9*(4), e95265. https://doi.org/10.1371/journal.pone.0095265

Willis, B. L., Gao, A., Leonard, D., DeFina, L. F., & Berry, J. D. (2012). Midlife fitness and the development of chronic conditions in later life. *Archives of Internal Medicine*, *172*(17), 1333–1340. https://doi.org/10.1001/archinternmed.2012.3400

Wolff, C. A., Lawrence, M. M., Porter, H., Zhang, Q., Reid, J. J., Laurin, J. L., Musci, R. v., Linden, M. A., Peelor, F. F., Wren, J. D., Creery, J. S., Cutler, K. J., Carson, R. H., Price, J. C., Hamilton, K. L., & Miller, B. F. (2020). Sex differences in changes of protein synthesis with rapamycin treatment are minimized when metformin is added to rapamycin. *GeroScience*, *43*, 809–828. https://doi.org/10.1007/s11357-020-00243-8

## SUPPORTING INFORMATION

Additional supporting information can be found online in the Supporting Information section at the end of this article.

**How to cite this article:** Bubak, M. P., Davidyan, A., O'Reilly, C. L., Mondal, S. A., Keast, J., Doidge, S. M., Borowik, A. K., Taylor, M. E., Volovičeva, E., Kinter, M. T., Britton, S. L., Koch, L. G., Stout, M. B., Lewis, T. L. Jr, & Miller, B. F. (2024). Metformin treatment results in distinctive skeletal muscle mitochondrial remodeling in rats with different intrinsic aerobic capacities. *Aging Cell*, *23*, e14235. https://doi.org/10.1111/acel.14235